[Electronic Supplementary Information to accompany *Chem. Sci.* manuscript # SC-EDG-07-2013-052010]

A dual approach to tuning the porosity of porous organic polymers: controlling the porogen size and supercritical CO_2 processing

Ryan K. Totten, Laura L. Olenick, Ye-Seong Kim, Sanjiban Chakraborty, Mitchell H. Weston, Omar K. Farha,* Joseph T. Hupp,* SonBinh T. Nguyen*

Department of Chemistry and the Institute for Catalysis in Energy Processes, Northwestern University, 2145 Sheridan Road, Evanston, Illinois 60208-3113, USA

Email: o-farha@northwestern.edu (O.K.F.), j-hupp@ northwestern.edu (J.T.H.), and stn@northwestern.edu (S.T.N.)

Table of Contents *Page number*

S1. General information. ^{1}H and ^{13}C NMR spectra were recorded on a Bruker Avance 500 (499.4 MHz for ^{1}H, 125.8 MHz for ^{13}C) spectrometer. ^{1}H NMR data are reported as follows: chemical shift (multiplicity (bs = broad singlet, s = singlet, d = doublet, t = triplet, q = quartet, and m = multiplet), coupling constant and integration). ^{1}H and ^{13}C chemical shifts are reported in ppm downfield from tetramethylsilane (TMS, δ scale) using the residual solvent resonances as internal standards.

^{1}H-^{13}C cross-polarization, magic angle spinning (CP-MAS) nuclear magnetic resonance spectra were recorded on a Varian VNMRS 400 MHz (400 MHz for ^{1}H, 100. MHz for ^{13}C) spectrometer (Varian, Inc., Palo Alto, CA, USA) equipped with a 5-mm HXY T3 PENCIL probe. The samples were packed into a standard 5-mm (external diameter) zirconia rotor with a volume of 160 μL and capped with a Teflon spacer. The spinning rate was at 10 kHz. ^{13}C NMR chemical shifts are reported in ppm downfield relative to tetramethylsilane (TMS) as zero ppm, calibrated using adamantane (38.3 ppm) as a secondary standard. All the spectra were acquired with neat powdered samples at room temperature. All the data were processed by VnmrJ software (Varian, Inc., Palo Alto, CA, USA) with a line broadening of 20 Hz.

Matrix-assisted laser desorption ionization time-of-flight (MALDI-ToF) mass spectra were recorded on a Bruker Autoflex III spectrometer using reflective positive MALDI ionization method with pyrene matrix. UV-vis spectra were obtained in $CHCl_3$ on a Varian Cary 500 spectrophotometer.

Inductively coupled plasma optical emission spectroscopy (ICP-OES) was conducted on a Varian Vista MPX ICP- OES instrument that is equipped to cover the spectral range from 175 to 785 nm. Samples (3 mg) were digested in conc. H_2SO_4:30% aq. H_2O_2 (3:1 v/v) and heated at 120 °C until the solution became clear and colorless. The clear solution was diluted to 5 vol% with deionized H_2O and analyzed for Sn (283.998 nm) content against standardized solutions containing 2, 5, 10, 20, and 30 ppm of Sn that were prepared from commercially available ICP standard solutions. Elemental analyses were provided by Atlantic Microlab, Inc. (Norcross, GA).

Quantification of the released axial ligands was carried out using gas chromatography (GC) performed on an Agilent Technologies 6890N Network GC system equipped with an FID detector and HP-5 capillary column (30 m × 320 μm × 0.25 μm film thickness). Analysis parameters were as followed: initial temperature = 50 °C, initial time = 3 minutes, ramp = 10 °C/min, final temperature = 200 °C, final time = 10 minutes. Elution times (min) = 10.4 (biphenyl, internal standard) 12.4 (3,5 di-*tert*-butyl benzaldehyde); 13.9 (3,5-diaminobenzoic acid); 14.5 (3,5 di-*tert*-butylbenzoic acid); released ligand concentration was calculated based on calibration curves using biphenyl as the external standard.

All N_2 adsorption and desorption measurements were performed on a Micromeritics Tristar 3020 system (Micromeretics, Norcross, GA) and measured at 77 K. Between 40-100 mg of samples were employed in each measurement and the data were analyzed using the ASAP 2020 software (Micromeretics, Norcross, GA). Before measurements, thermally activated

samples were degassed for 12 h at 150 ºC under high vacuum (< 10^{-4} bar). For the supercritical CO_2 processed samples, the samples were degassed under vacuum for an extra ½ h prior to measurements (the standard degas period on the Tristar 3020 instrument was 30 minutes). The specific surface areas for N_2 were calculated using the Brunauer-Emmet-Teller (BET) model in the range of $0.01 < P/P_0 < 0.1$ for type I isotherms and $0.01 < P/P_0 < 0.2$ for type II isotherms. The pore size distributions were calculated from the adsorption-desorption isotherms by density functional theory (DFT) in the range of $5.0 \times 10^{-5} < P/P_0 > 0.95$. The pore size distributions obtained were calculated using the slit-pore NLDFT model.

Pycnometer measurements were carried out at 25 °C on a Micromeritics AccuPyc II 1340 Pycnometer (Micrometetics, Norcross, GA).

Scanning electron microscopy (SEM) images were obtained using a Hitachi SU8030 scanning electron microscope (Hitachi High Technologies America, Inc. Dallas, TX) with an acceleration voltage of 20 kV. The samples were finely grounded and dispersed onto a double sticky carbon tape (Ted Pella Inc., Redding, CA) attached to a flat aluminium sample holder. The samples were then coated with a gold-palladium film of thickness ~ 30 nm to facilitate conduction using a Denton III Desk sputter coater (Denton Vacuum, LLC – USA, Moorestown, NJ) operating under argon atmosphere at 25 °C and ~30 mTorr.

S2. General procedures and materials. All air- or water-sensitive reactions were carried out under nitrogen using oven-dried glassware. All synthetic experiments concerning porphyrin and porphyrin derivatives were carried out under light-deficient conditions: the hood lights were turned off and the reaction flasks are covered with aluminum foil to further minimize light exposure. Isolated porphyrin products were stored at low temperatures (-10 °C) in foil-covered vials. All flash-chromatography was carried out using silica gel (MP Silitech 60-200 mesh) under a positive pressure of nitrogen, unless otherwise noted. Analytical thin layer chromatography (TLC) was performed using glass-backed silica gel 60 F_{254} plates (Merck EMD-571507). Visualization of the TLC results was achieved by observation under UV light (254 nm).

Tetrahydrofuran and dichloromethane (Fisher Scientific) were dried over neutral alumina in a Dow-Grubbs solvent system[S1] installed by Glass Contours (now JC Meyer Solvent Systems, Laguna Beach, CA, USA). ACS reagent-grade aqueous ammonium hydroxide (28.0-30.0 wt% NH_3 content) was purchased from Fisher Scientific (Hampton, NH, USA). All other reagents were purchased from the Aldrich Chemical Company (Milwaukee, WI, USA) and used without further purification, unless otherwise noted. Deuterated solvents were purchased from Cambridge Isotope Laboratories (Andover, MA, USA) and used without further purification. 5,15-*Bis*(pentafluorophenyl)-10,20-*bis*(4-ethynylphenyl)porphyrin[S2] and *tetrakis*(4-ethynylphenyl)methane[S3] were synthesized according to published procedures.

S3. Preparation of 3,5-*bis*[(3,5-di-*tert*-butyl)benzylideneamino]benzoic acid.

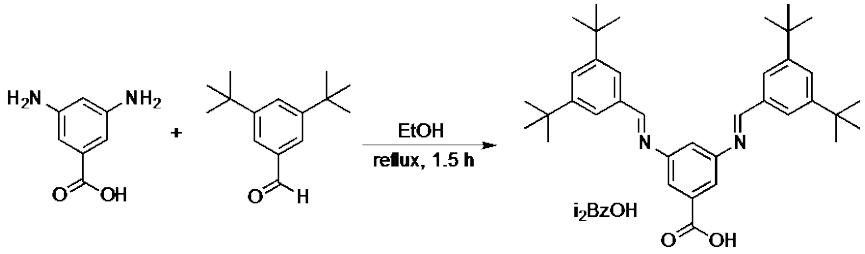

3,5-*Bis*[(3,5-di-*tert*-butyl)benzylideneamino]benzoic acid (i_2BzOH, the notation i represents the imine group). 3,5-Diaminobenzoic acid (0.5 g, 3.3 mmol) and 3,5-di-*tert*-butyl benzaldehyde (1.4 g, 6.6 mmol) were combined with ethanol (25 mL) in a 100 mL round-bottom flask equipped with a magnetic stir bar and a water-cooled reflux condenser. The resulting mixture was allowed to stir at reflux for 1.5 h before being evaporated to dryness using a rotary evaporator. The remaining crude product was redissolved in CH_2Cl_2 (100 mL), dried over $MgSO_4$, filtered, and evaporated to dryness under reduced pressure to afford the product as a light brown solid (1.8 g, 3.3 mmol, 99% yield) that can be used without further purification. ^{1}H NMR (499.4 MHz, $CDCl_3$): δ 1.4 (s, 36H, C(CH_3)$_3$), 7.40 (s, 1H, Ar-*H*), 7.60 (s, 2H, Ar-*H*), 7.80 (d, *J* = 2.0 Hz, 4H, Ar-*H*), 7.85 (d, *J* = 2.0 Hz, 2H, Ar-*H*), 8.57 (s, 2H, NC*H*). {^{1}H}^{13}C NMR (125.8 MHz, $CDCl_3$): δ 31.4, 35.0, 113.8, 120.9, 123.6, 126.3, 132.5, 151.6, 157.5, 163.2, 171.9, 193.4.

S4. Preparation of Sn(porphyrin) monomers. In the current manuscript, we chose to work with the pentafluorophenyl-substituted porphyrin simply for synthetic reasons. The pentafluorophenyl dipyrromethane starting material is very easy to obtain and handle as it can be crystallized directly from the crude reaction mixture and easily recovered by filtration to give pure product. In contrast, the purification of phenyl dipyrromethane requires tedious chromatography prior to recrystallization.[S4]

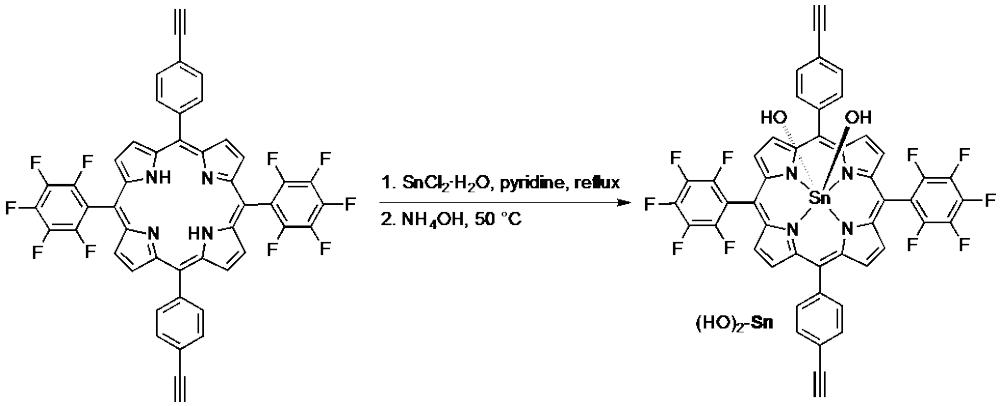

[5,15-*Bis*(pentafluorophenyl)-10,20-*bis*(4-ethynylphenyl)porphyrinato]tin(IV) dihydroxide ($(HO)_2$-Sn). 5,15-*Bis*(pentafluorophenyl)-10,20-*bis*(4-ethynylphenyl)porphyrin (1.6 g, 1.9 mmol) and $SnCl_2 \cdot 2H_2O$ (6.4 g, 28.5 mmol) were combined with pyridine (200 mL) in a 500 mL round-bottom flask equipped with a magnetic stir bar and a water-cooled reflux condenser. The resulting mixture was allowed to stir under reflux for 3 h before it was cooled to 50 °C and treated with ACS reagent-grade aqueous NH_4OH (50 mL). After stirring overnight, the reaction mixture was allowed to cool to room temperature then filtered through a Buchner funnel to remove the excess tin salts. The product was precipitated by pouring the filtrate into an Erlenmeyer flask containing water (1 L) and isolated by filtration through a Buchner funnel. The product-containing filter cake was dissolved in CH_2Cl_2 (300 mL), washed with water (3 × 200 mL), dried over $MgSO_4$, filtered, and evaporated to dryness under reduced pressure to afford the product as a purple solid (1.6 g, 1.6 mmol, 85% yield). ^{1}H NMR (499.4 MHz, $CDCl_3$): δ 3.39 (s, 2H, CC*H*), 7.80 (d, J = 8.0 Hz, 4H, Ar-*H*), 8.30 (d, J = 7.5 Hz, 4H, Ar-*H*), 9.24 (d, J = 4.5 Hz, 4H, β-*H*), 9.28 (d, J = 4.5 Hz, 4H, β-*H*). $\{^1H\}^{13}C$ NMR (125.8 MHz, $CDCl_3$): δ 29.8, 53.5, 78.8, 83.4, 100.5, 116.3, 120.6, 122.2, 130.8, 134.5, 141.8, 145.6, 147.6. MALDI-ToF MS (reflective positive mode): Calcd for $C_{48}H_{20}F_{10}N_4O_2Sn$: 993.39, found: *m/z* 976.78 $[M\text{-}OH]^+$. UV-vis: (nm, ($\varepsilon \times 10^4$ /$M^{-1}cm^{-1}$)) 419 (40.3), 509 (0.3), 555 (1.1), 594 (0.4). See Fig. S1 for the NMR spectra.

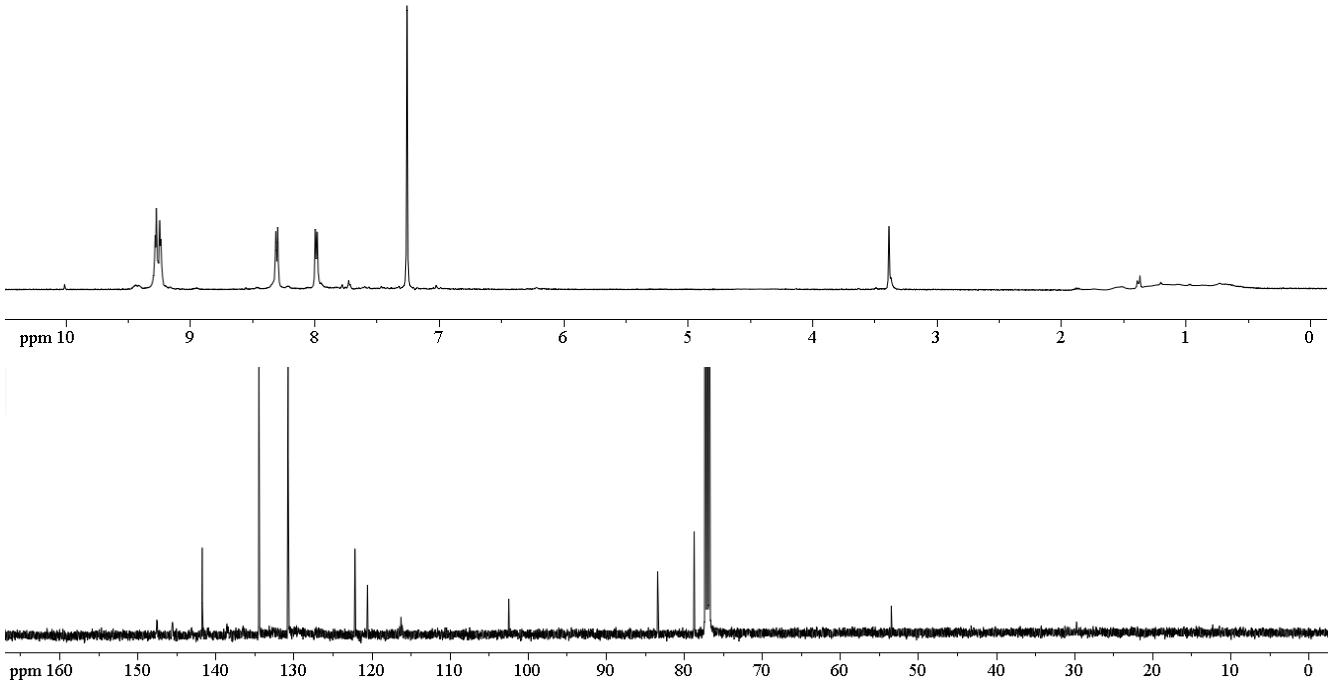

Figure S1. The ^{1}H (top) and ^{13}C (bottom) NMR spectra for [5,15-*bis*(pentafluorophenyl)-10,20-*bis*(4-ethynylphenyl)porphyrinato]tin(IV) dihydroxide.

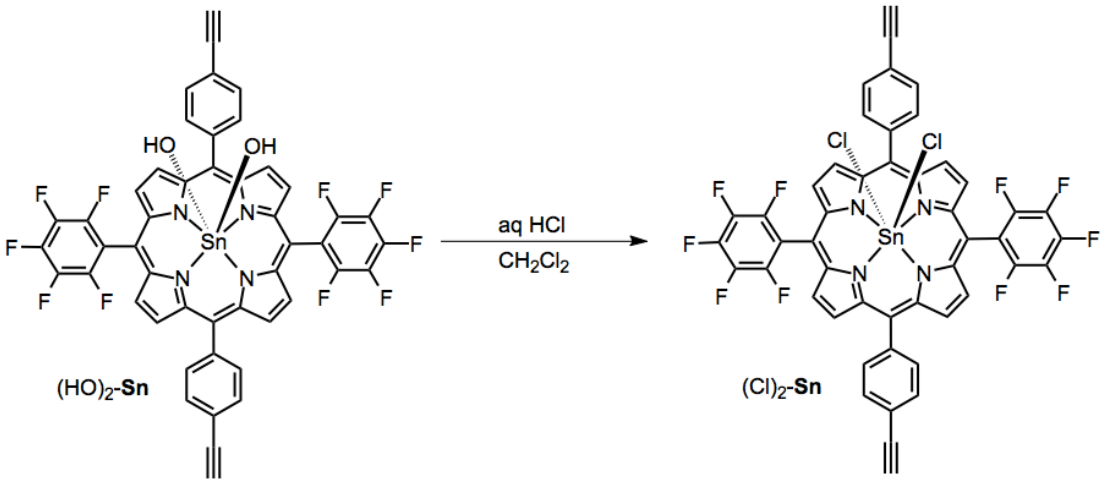

[5,15-*Bis*(pentafluorophenyl)-10,20-*bis*(4-ethynylphenyl)porphyrinato]tin(IV) dichloride ($(Cl)_2$-Sn). $(HO)_2$-**Sn** (100 mg, 0.1 mmol) was combined with CH_2Cl_2 (50 mL) in a 250 mL separatory funnel and washed with 1 M HCl (3 × 30 mL). The organic layer was then washed with water (3 × 30 mL), dried over $MgSO_4$, filtered, and evaporated to dryness under reduced pressure to afford the product as a purple solid (100 mg, 0.1 mmol, 97% yield). ^{1}H NMR (499.4 MHz, $CDCl_3$): δ 3.40 (s, 2H, CC*H*), 8.00 (d, *J* = 7.5 Hz, 4H, Ar-*H*), 8.31 (d, *J* = 7.5 Hz, 4H, Ar-*H*), 9.21 (d, *J* = 4.5 Hz, 4H, β-*H*), 9.31 (d, *J* = 4.5 Hz, 4H, β-*H*). {^{1}H}^{13}C NMR (125.8 MHz, $CDCl_3$): δ 30.1, 53.8, 79.8, 83.3, 104.1, 122.1, 123.5, 131.4, 131.7, 134.6, 135.2, 140.5, 146.2, 147.1. MALDI-ToF MS (reflective positive mode): Calcd for $C_{48}H_{18}Cl_2F_{10}N_4Sn$: 1030.28, found: *m/z* 995.54 $[M\text{-}Cl]^+$. UV-vis: (nm, (ε ×10^4 /M^{-1}cm^{-1})) 420 (39.8), 510 (0.2), 556 (0.9), 594 (0.4). See Fig. S2 for the NMR spectra.

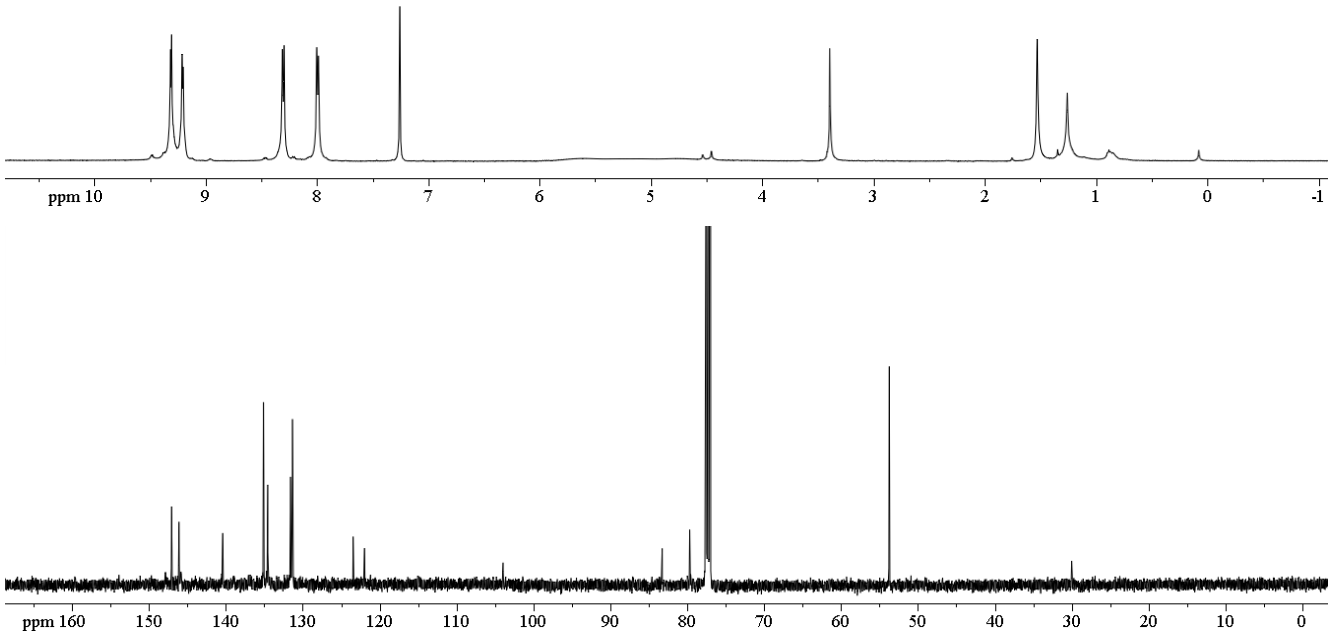

Figure S2. The ^{1}H (top) and ^{13}C (bottom) NMR spectra for [5,15-*bis*(pentafluorophenyl)-10,20-*bis*(4-ethynylphenyl)porphyrinato]tin(IV) dichloride.

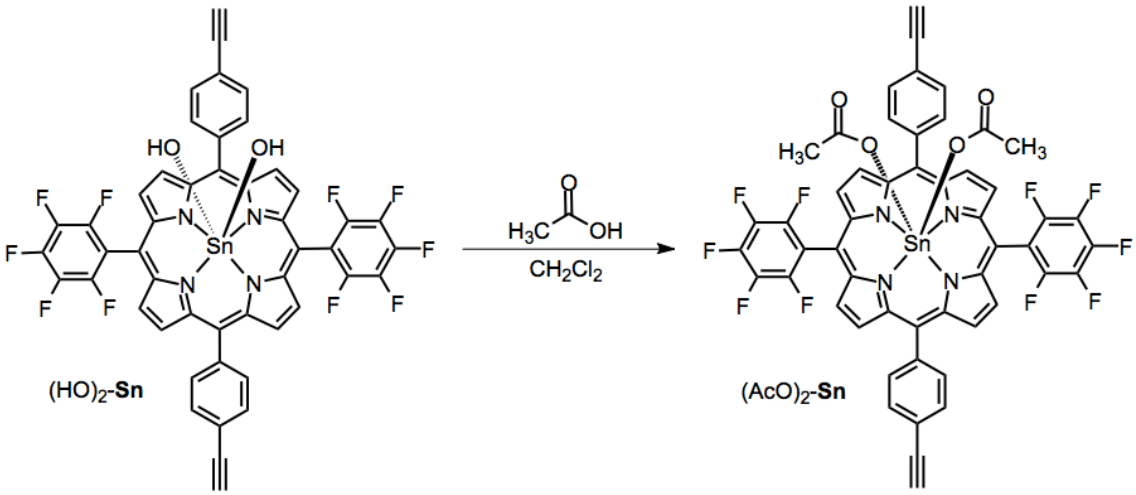

[5,15-*Bis*(pentafluorophenyl)-10,20-*bis*(4-ethynylphenyl)porphyrinato]tin(IV) diacetate ($(AcO)_2$-Sn). $(HO)_2$-**Sn** (100 mg, 0.1 mmol) and acetic acid (30 μL, 0.5 mmol) were combined with CH_2Cl_2 (30 mL) in a 100 mL round-bottom flask equipped with a magnetic stir bar. The resulting mixture was allowed to stir under N_2 for 12 h at room temperature before being evaporated to dryness using a rotary evaporator. The remaining crude product was redissolved in a minimal amount of CH_2Cl_2 (3 mL) and the product was precipitated out of this solution with hexanes (100 mL). After filtration and air-dried, the pure product was obtained as a purple solid (100 mg, 0.09 mmol, 92% yield). ^{1}H NMR (499.4 MHz, $CDCl_3$): δ -1.01 (s, 6H, CO_2CH_3), 3.38 (s, 2H, CC*H*), 8.00 (d, J = 8.0 Hz, 4H, Ar-*H*), 8.32 (d, J = 8.0 Hz, 4H, Ar-*H*), 9.18 (d, J = 5.0 Hz, 4H, β-*H*), 9.30 (d, J = 5.0 Hz, 4H, β-*H*). $\{^1H\}^{13}C$ NMR (125.8 MHz, $CDCl_3$): δ 20.7, 79.5, 83.5, 103.9, 122.8, 123.2, 131.2, 131.4, 134.6, 134.9, 140.9, 146.7, 148.2, 168.9. MALDI-ToF MS (reflective positive mode): Calcd for $C_{52}H_{24}F_{10}N_4O_4Sn$: 1077.47, found: *m/z* 1019.44 $[M\text{-acetate}]^+$. UV-vis: (nm, ($\varepsilon \times 10^4$ /$M^{-1}cm^{-1}$)) 420 (42.1), 510 (0.3), 556 (1.1), 594 (0.4). See Fig. S3 for the NMR spectra.

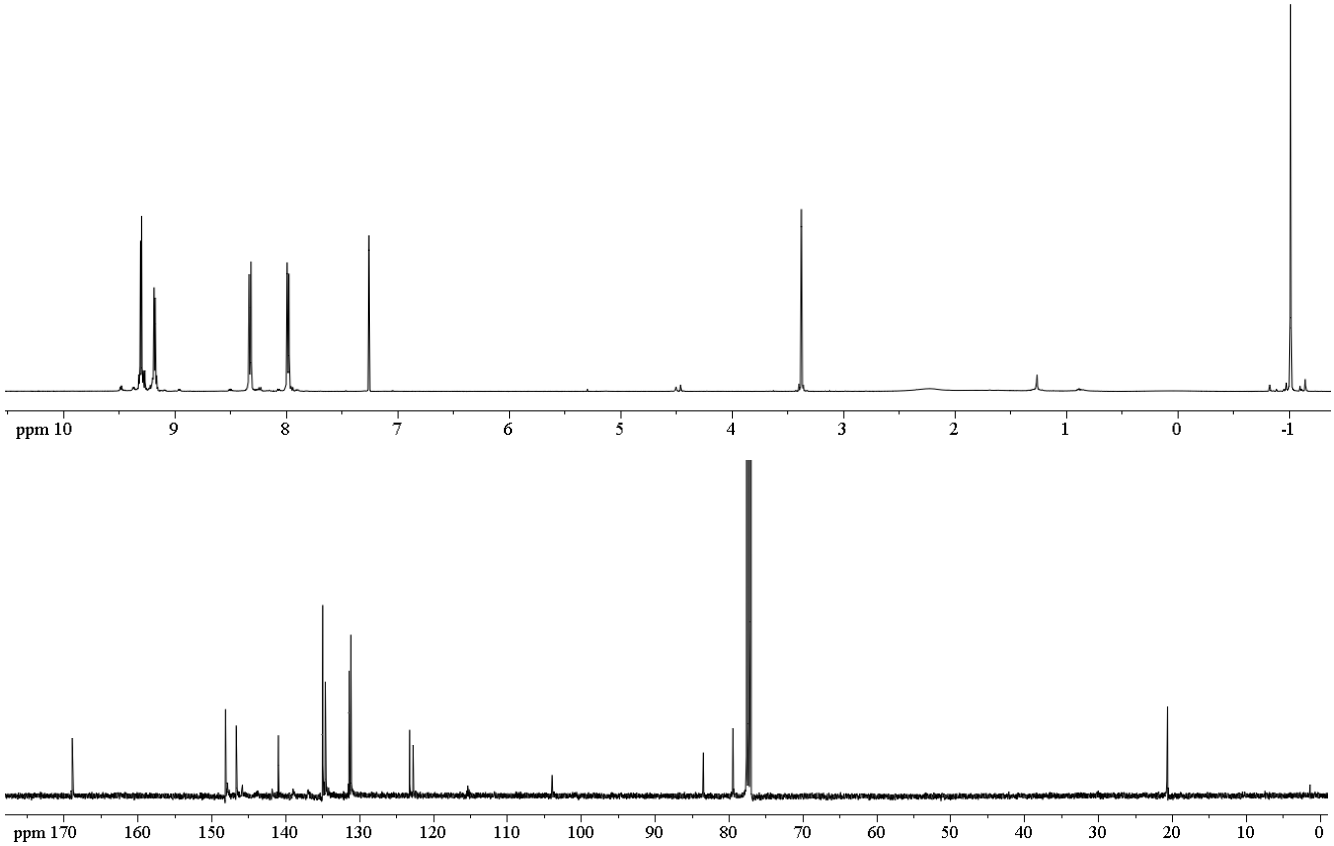

Figure S3. The ^{1}H (top) and ^{13}C (bottom) NMR spectra for [5,15-*bis*(pentafluorophenyl)-10,20-*bis*(4-ethynylphenyl)porphyrinato]tin(IV) diacetate.

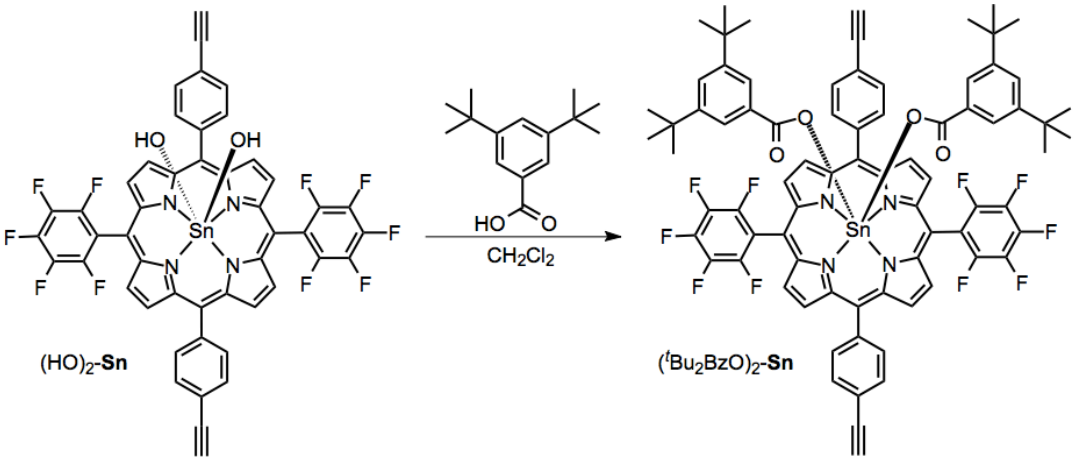

[5,15-*Bis*(pentafluorophenyl)-10,20-*bis*(4-ethynylphenyl)porphyrinato]tin(IV) *bis*(3,5-di-*tert*-butylbenzoate) ((^{t}Bu$_2$BzO)$_2$-Sn). (HO)$_2$-**Sn** (100 mg, 0.1 mmol) and 3,5-di-*tert*-butylbenzoic acid (59 mg, 0.25 mmol) were combined with CH_2Cl_2 (30 mL) in a 100 mL round-bottom flask equipped with a magnetic stir bar. The resulting mixture was allowed to stir under N_2 for 12 h at room temperature before being evaporated to dryness using a rotary evaporator. The remaining crude product was redissolved in a minimal amount of CH_2Cl_2 (3 mL) and the product was precipitated out of solution with hexanes (100 mL). The pure product was isolated by filtration as a purple solid (126 mg, 0.09 mmol, 88% yield). ^{1}H NMR (499.4 MHz, $CDCl_3$): δ 0.64 (s, 36H, C(C*H*$_3$)$_3$), 3.37 (s, 2H, CC*H*), 4.77 (s, 4H, Ar-*H*), 6.67 (s, 2H, Ar-*H*), 7.94 (d, *J* = 8.0 Hz, 4H, Ar-*H*), 8.23 (d, *J* = 8.0 Hz, 4H, Ar-*H*), 9.26 (s, 8H, β-*H*). {^{1}H}^{13}C NMR (125.8 MHz, $CDCl_3$): δ 14.1, 30.8, 31.4, 33.9, 34.9, 62.5, 79.0, 121.4, 122.7, 123.8, 124.4, 130.8, 131.6, 133.9, 134.7, 134.9, 140.8, 145.8, 146.6, 146.9, 148.6, 151.2, 163.3. MALDI-ToF MS (reflective positive mode): Calcd for $C_{78}H_{60}F_{10}N_4O_4Sn$: 1426.03, found: *m/z* 1192.49 [M - 3,5-di-*tert*-butyl benzoic acid]$^+$. UV-vis: (nm, (ε ×10^4 /M^{-1}cm^{-1})) 420 (41.9), 510 (0.3), 556 (1.2), 594 (0.4). See Fig. S4 for the NMR spectra.

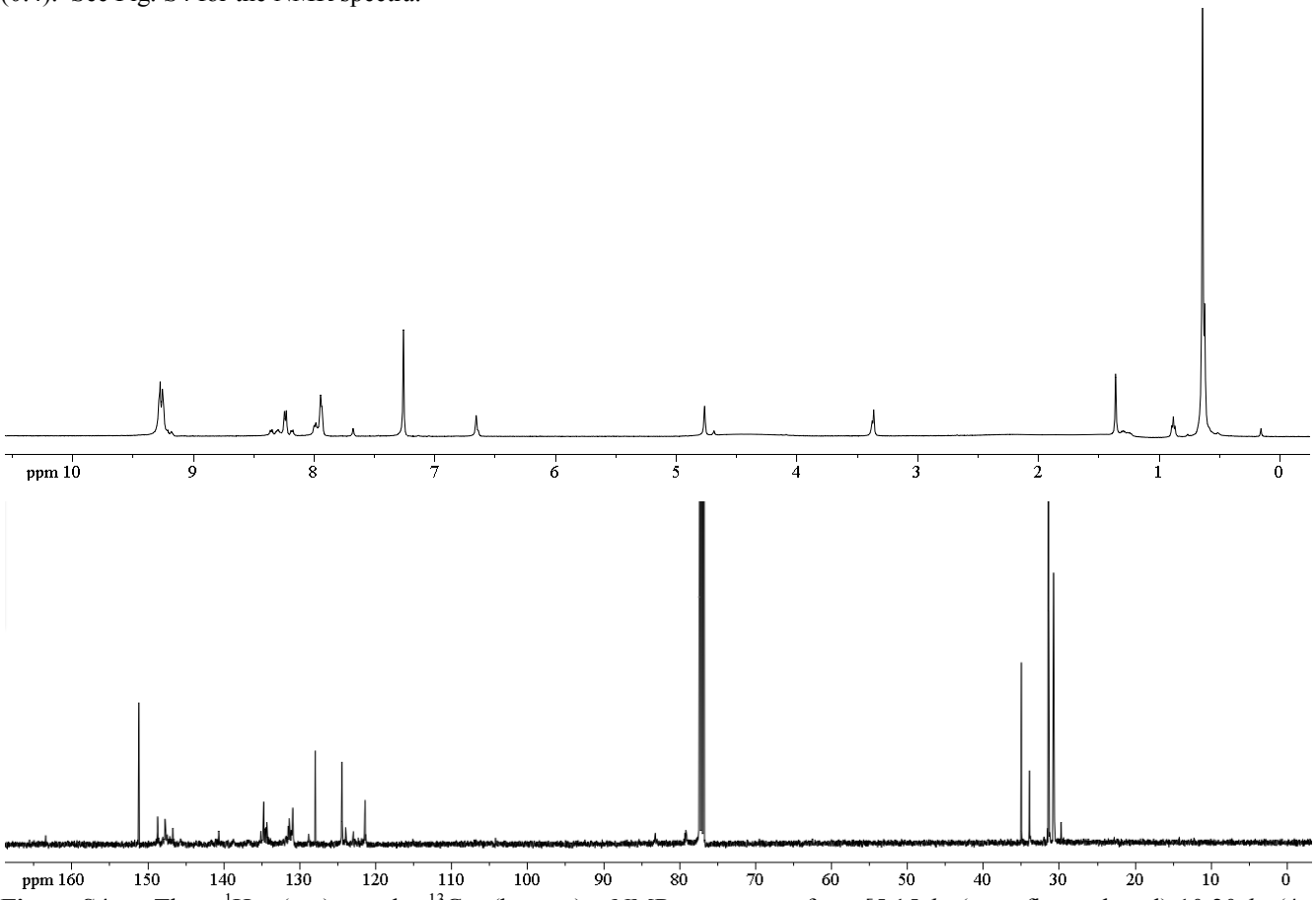

Figure S4. The ^{1}H (top) and ^{13}C (bottom) NMR spectra for [5,15-*bis*(pentafluorophenyl)-10,20-*bis*(4-ethynylphenyl)porphyrinato]tin(IV) *bis*(3,5-di-*tert*-butylbenzoate).

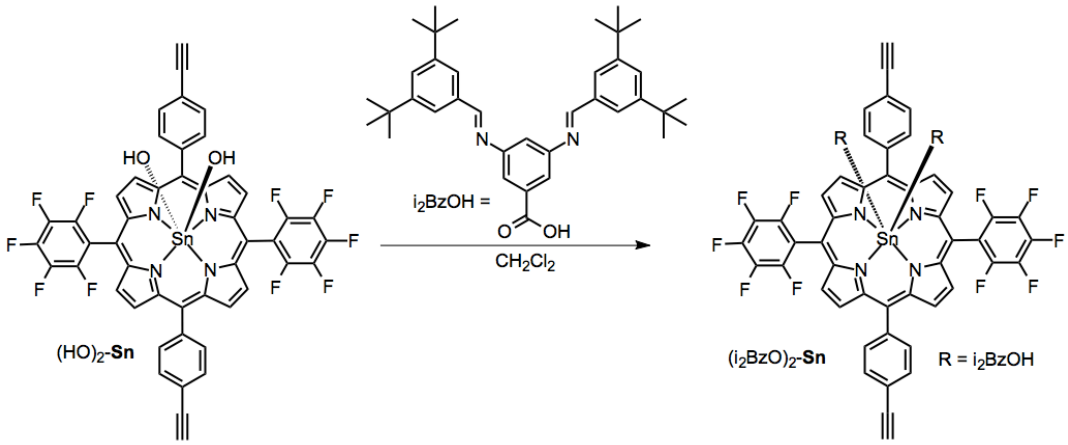

[5,15-*Bis*(pentafluorophenyl)-10,20-*bis*(4-ethynylphenyl)porphyrinato]tin(IV) *bis*(3,5-*bis*[(3,5-di-*tert*-butyl)benzylideneamino]benzoic acid) ($(i_2BzO)_2$-Sn)). $(HO)_2$-**Sn** (100 mg, 0.1 mmol) and i_2BzOH (138 mg, 0.25 mmol) were combined with CH_2Cl_2 (30 mL) in a 100 mL round-bottom flask equipped with a magnetic stir bar. The resulting mixture was allowed to stir under N_2 for 12 h at room temperature before being evaporated to dryness using a rotary evaporator. The remaining crude product was redissolved in a minimal amount of CH_2Cl_2 (3 mL) and the product was precipitated out of solution with hexanes (100 mL). Pure product was isolated by filtration as a purple solid (165 mg, 0.08 mmol, 80% yield). ^{1}H NMR (499.4 MHz, $CDCl_3$): δ 1.35 (m, 72H, C(C*H*$_3$)$_3$), 3.31 (s, 2H, CC*H*), 4.52 (s, 4H, Ar-*H*), 6.46 (s, 2H, Ar-*H*), 7.51 (s, 4H, Ar-*H*), 7.55 (s, 2H, Ar-*H*), 7.60 (s, 2H, Ar-*H*), 7.62 (s, 2H, Ar-*H*), 7.70 (s, 4H, Ar-*H*), 7.75 (s, 2H, Ar-*H*), 7.80 (s, 2H, Ar-*H*) 8.57 (s, 2H, NC*H*), 8.94 (d, *J* = 4.5 Hz, 4H, β-*H*), 9.05 (d, *J* = 4.5 Hz, 4H, β-*H*). {^{1}H}^{13}C NMR (125.8 MHz, $CDCl_3$): δ 29.9, 30.8, 31.4, 34.1, 35.1, 79.0, 83.5, 103.4, 121.3, 121.6, 122.4, 124.5, 128.2, 130.8, 133.9, 141.5, 147.9, 148.8, 149.0, 151.3, 162.9, 172.3. MALDI-ToF MS (reflective positive mode): Calcd for $C_{119}H_{106}F_{10}N_4O_4Sn$: 2020.86, found: *m/z* 1511.39 [M - 3,5-*bis*[(3,5-di-*tert*-butyl)benzylideneamino]benzoic acid]$^+$. UV-vis: (nm, (ε ×10^4 /M^{-1}cm^{-1})) 420 (40.3), 510 (0.3), 556 (1.0), 594 (0.4). See Fig. S5 for the NMR spectra.

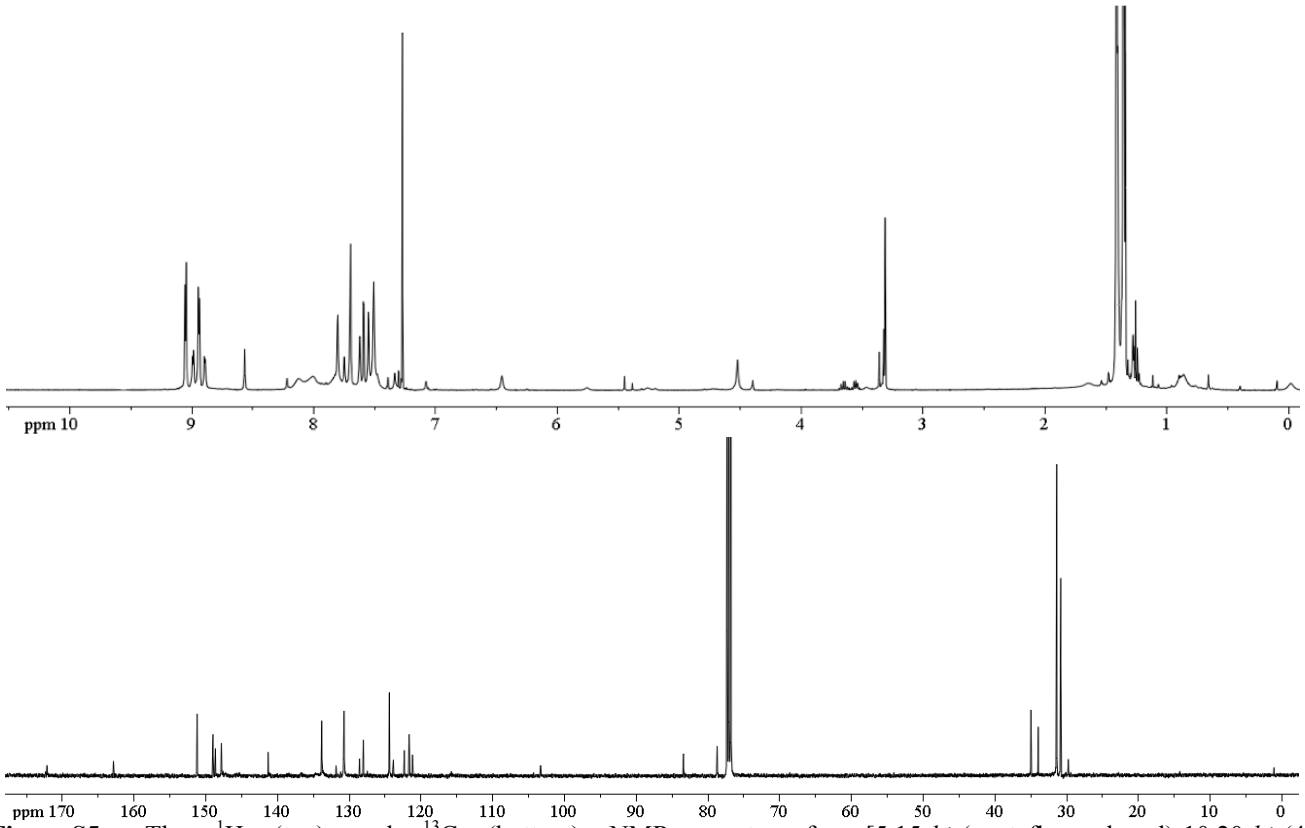

Figure S5. The ^{1}H (top) and ^{13}C (bottom) NMR spectra for [5,15-*bis*(pentafluorophenyl)-10,20-*bis*(4-ethynylphenyl)porphyrinato]tin(IV) *bis*(3,5-bis(3,5-di-*tert*-butylbenzylideneamino)benzoic acid).

S5. Preparation of thermally activated Sn-PPOPs.

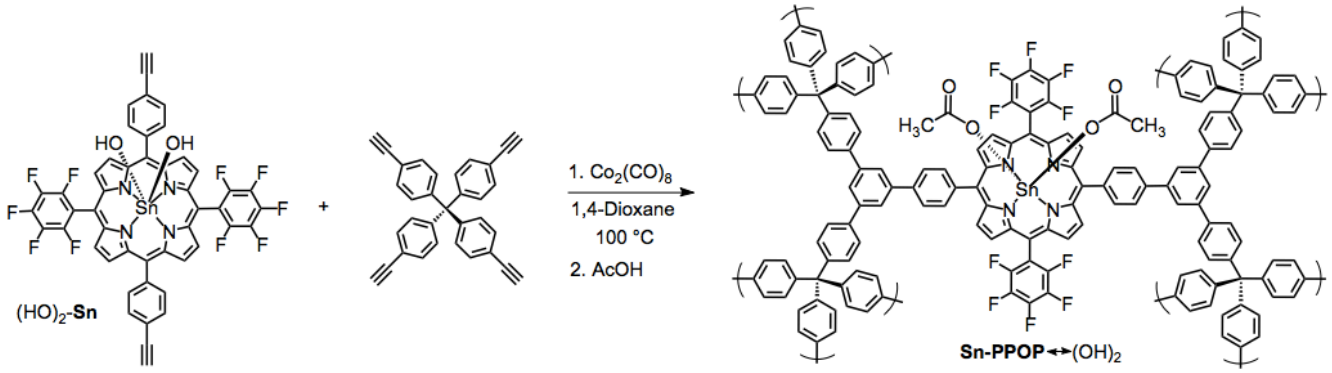

Sn-PPOP↔(OH)$_2$. In a nitrogen-filled glovebox, a 20 mL microwave vial (capacity designates the amount of solution that can be safely loaded) equipped with a magnetic stir bar was charged with (HO)$_2$-**Sn** (100 mg, 0.1 mmol), *tetrakis*(4-ethynylphenyl)methane (21 mg, 0.5 mmol), and dry 1,4-dioxane (12 mL). $Co_2(CO)_8$ (17 mg, 0.05 mmol) was then added to the resulting solution and the microwave vial was sealed with a crimp cap. The vial was removed from the glovebox and placed into a 100 ºC oil bath where the reaction mixture was allowed to stir for 1.5 h. The solution thickened and precipitates were observed after about 5 min; after 10 min, significant gelation could be observed. After 1.5 h, the vial was removed from the oil bath and cooled down slightly; the crimp cap was removed and acetic acid (1 mL) was then added to the mixture. A spatula was used to broken up the gel into smaller particles; the vial was crimp-capped again, put back into the 100 ºC oil bath, and kept there while stirring for 1 h. The hot reaction mixture was then filtered through a fine-fritted glass funnel and the remaining purple solid was washed with THF (30 mL), MeOH (30 mL), and H_2O (30 mL). Removal of solvent under vacuum at 150 ºC gave a purple solid (125 mg, 98% yield). Anal.: Calcd for $(C_{137}H_{68}F_{20}N_8O_8Sn_2)_n$: C, 63.99; H, 2.67; N, 4.36. Found: C, 58.17; H, 2.32; N, 4.09. ICP-OES: Calcd for $(C_{137}H_{68}F_{20}N_8O_8Sn_2)_n$: 9.2 wt% Sn. Found: 9.1 wt% Sn. See Fig. S6 for the solid-state ^{1}H-^{13}C CP-MAS NMR spectrum.

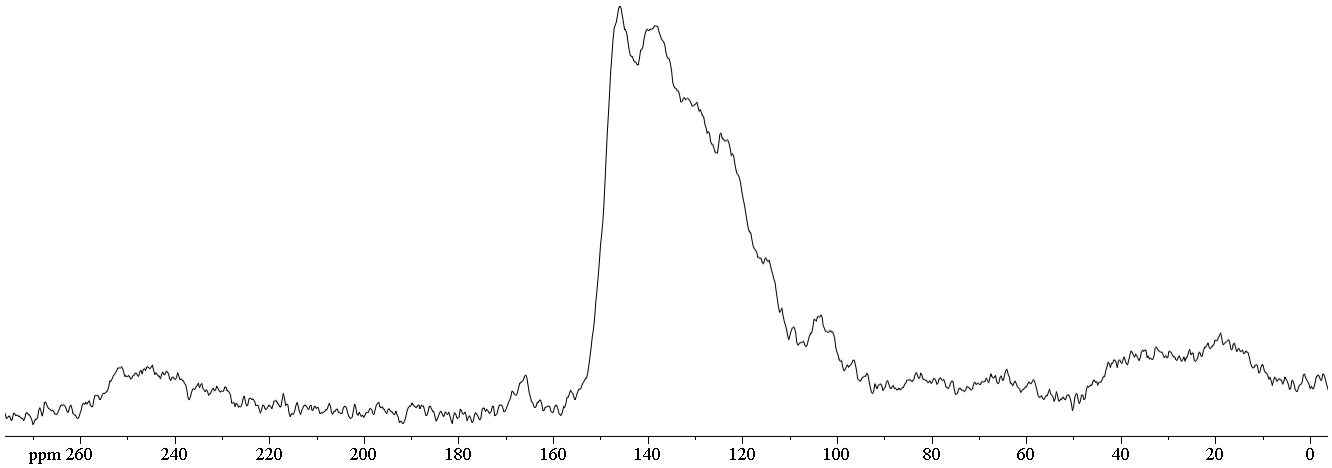

Figure S6. The solid-state ^{1}H-^{13}C CP-MAS NMR spectrum of **Sn-PPOP↔**(OH)$_2$ recorded at a MAS rate of 10 kHz.

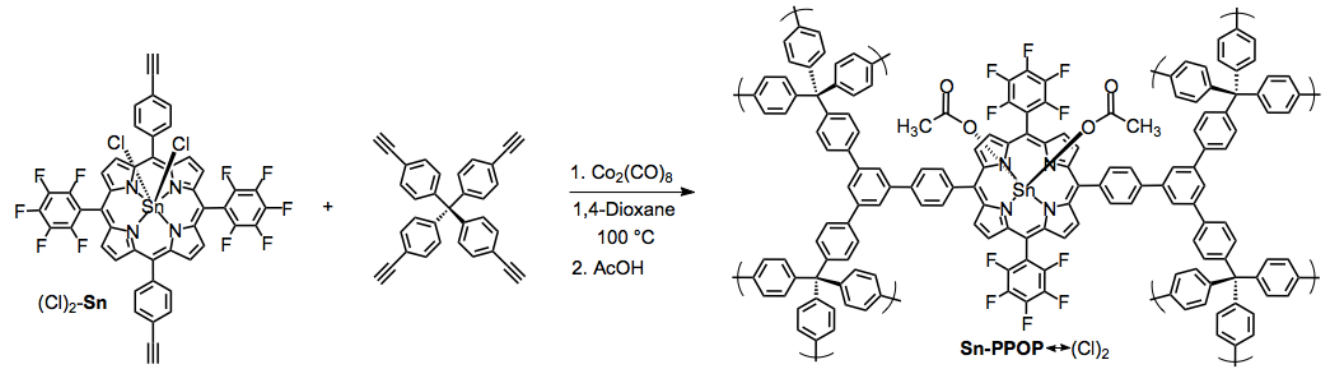

Sn-PPOP↔(Cl)$_2$. **Sn-PPOP↔**(Cl)$_2$ was synthesized under the same protocol and scale as described for **Sn-PPOP↔**(OH)$_2$. Product was isolated as a purple solid (124 mg, 97% yield). Anal.: Calcd for $(C_{137}H_{68}F_{20}N_8O_8Sn_2)_n$: C,

63.99; H, 2.67; N, 4.36. Found: C, 56.44; H, 2.06; N, 4.09. ICP-OES: Calcd for $(C_{137}H_{68}F_{20}N_8O_8Sn_2)_n$: 9.2 wt% Sn. Found: 9.1 wt% Sn. See Fig. S7 for the solid-state ^1H-^{13}C CP-MAS NMR spectrum.

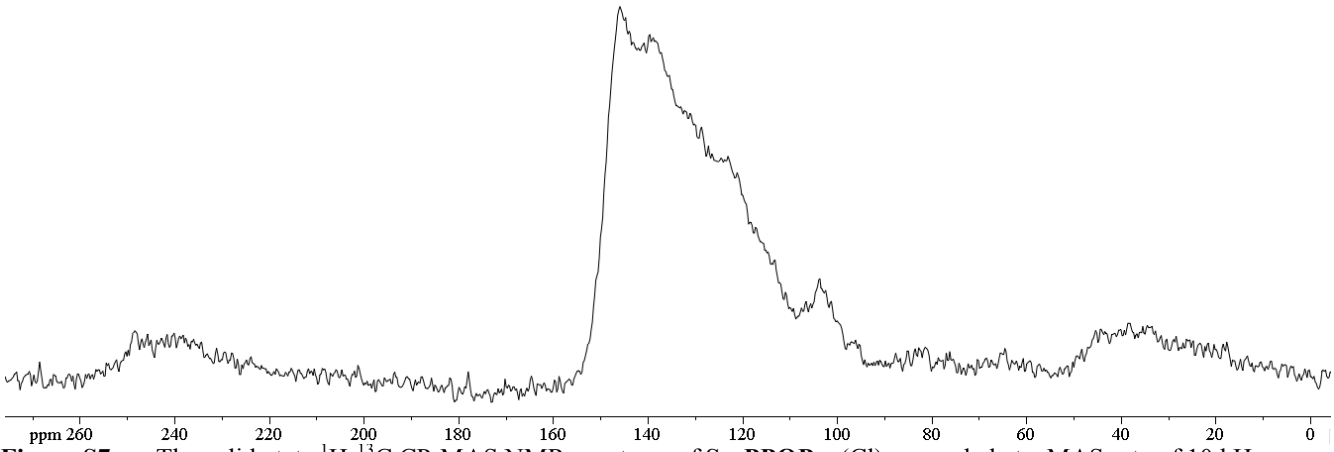

Figure S7. The solid-state ^1H-^{13}C CP-MAS NMR spectrum of **Sn-PPOP↔**$(Cl)_2$ recorded at a MAS rate of 10 kHz.

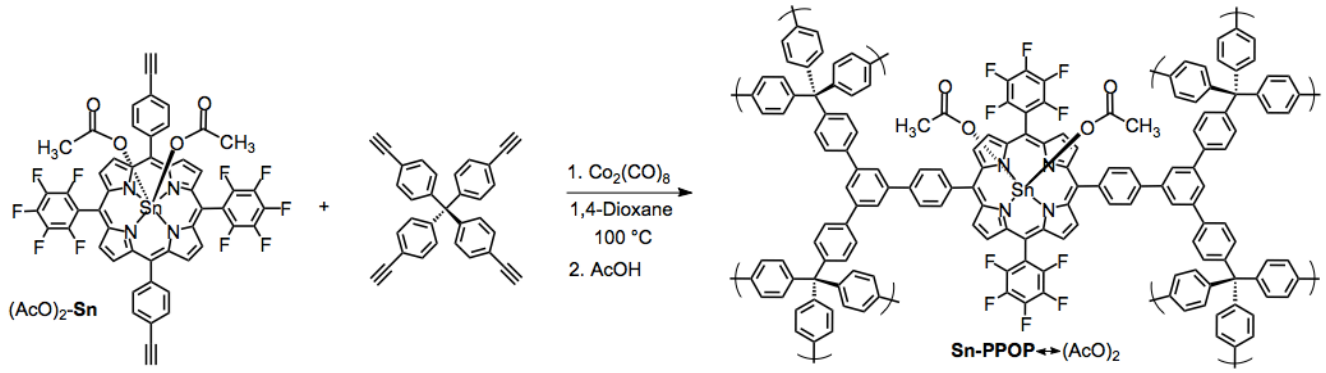

Sn-PPOP↔(AcO)$_2$. **Sn-PPOP↔**$(AcO)_2$ was synthesized under the same protocol and scale as described for **Sn-PPOP↔**$(OH)_2$. Product was isolated as a purple solid (125 mg, 98% yield). Anal.: Calcd for $(C_{137}H_{68}F_{20}N_8O_8Sn_2)_n$: C, 63.99; H, 2.67; N, 4.36. Found: C, 58.35; H, 2.34; N, 4.07. ICP-OES: Calcd for $(C_{137}H_{68}F_{20}N_8O_8Sn_2)_n$: 9.2 wt% Sn. Found: 9.2 wt% Sn. See Fig. S8 for the solid-state ^1H-^{13}C CP-MAS NMR spectrum.

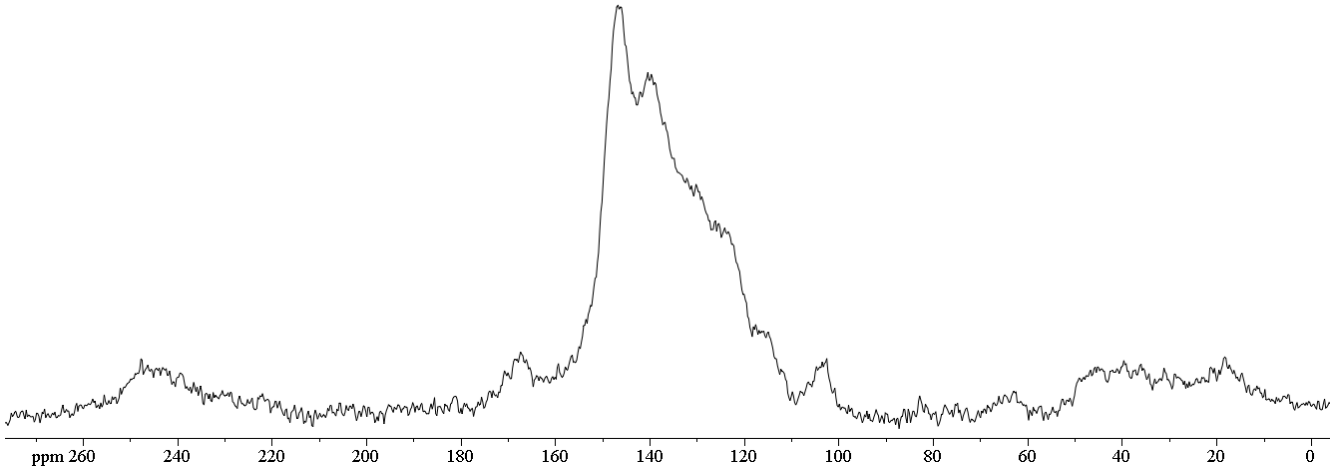

Figure S8. The solid-state ^1H-^{13}C CP-MAS NMR spectrum of **Sn-PPOP↔**$(AcO)_2$ recorded at a MAS rate of 10 kHz.

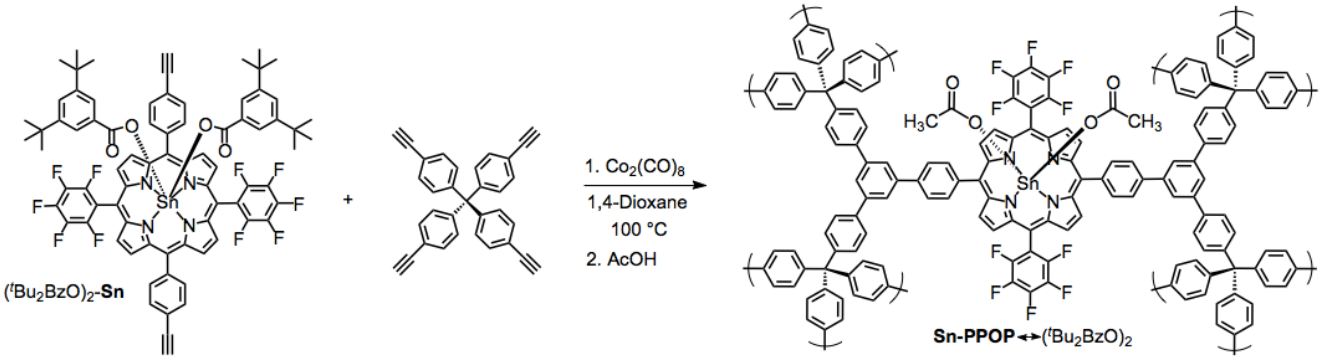

Sn-PPOP↔(^{t}Bu$_2$BzO)$_2$. **Sn-PPOP↔**(^{t}Bu$_2$BzO)$_2$ was synthesized under the same protocol and scale as described for **Sn-PPOP↔**(OH)$_2$. The complete release of the 3,5-di-^{t}butyl benzoic acid ligand during the acetic acid workup was observed by GC analysis against a biphenyl external standard (see procedure below). Product was isolated as a purple solid (124 mg, 97% yield). Anal.: Calcd for $(C_{137}H_{68}F_{20}N_8O_8Sn_2)_n$: C, 63.99; H, 2.67; N, 4.36. Found: C, 61.38; H, 2.87; N, 4.40. ICP-OES: Calcd for $(C_{137}H_{68}F_{20}N_8O_8Sn_2)_n$: 9.2 wt% Sn. Found: 9.4 wt% Sn. See Fig. S9 for the solid-state ^{1}H-^{13}C CP-MAS NMR spectrum.

The mother liquor that was recovered after the acetic acid wash was concentrated to dryness under rotary evaporation. The remaining residue was dissolved in CH_2Cl_2 (10 mL) and an aliquot was subsequently withdrawn (100 μL) and diluted with a solution of biphenyl in CH_2Cl_2 (1 mL of a 2 mM solution). The percentage of 3,5-di-*tert*-butyl benzoate ligand removed from the acetic acid wash was determined to be 96% (calculated based on a calibration curve using biphenyl as the external standard)

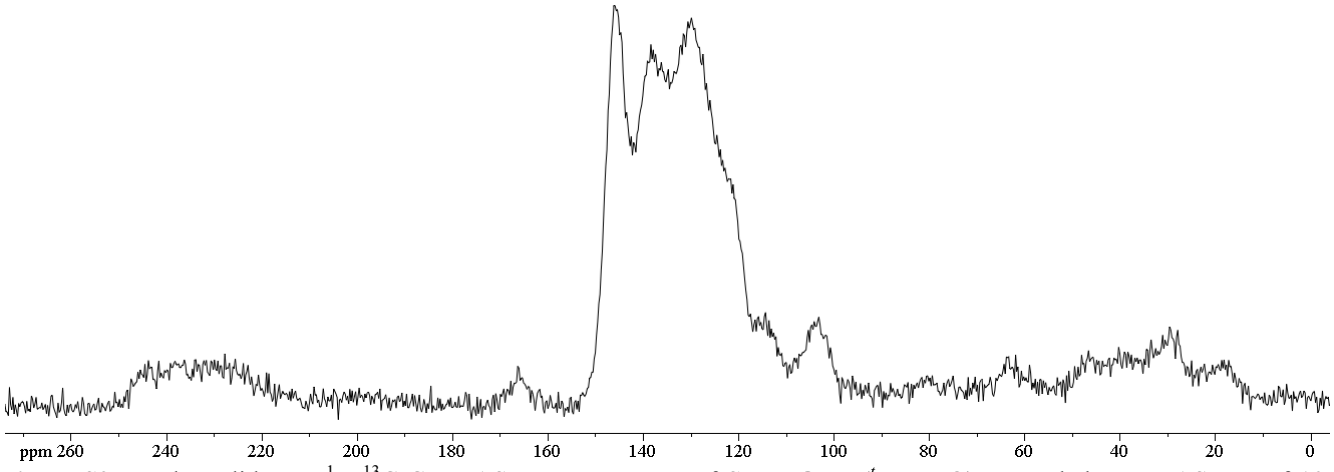

Figure S9. The solid-state ^{1}H-^{13}C CP-MAS NMR spectrum of **Sn-PPOP↔**(^{t}Bu$_2$BzO)$_2$ recorded at a MAS rate of 10 kHz.

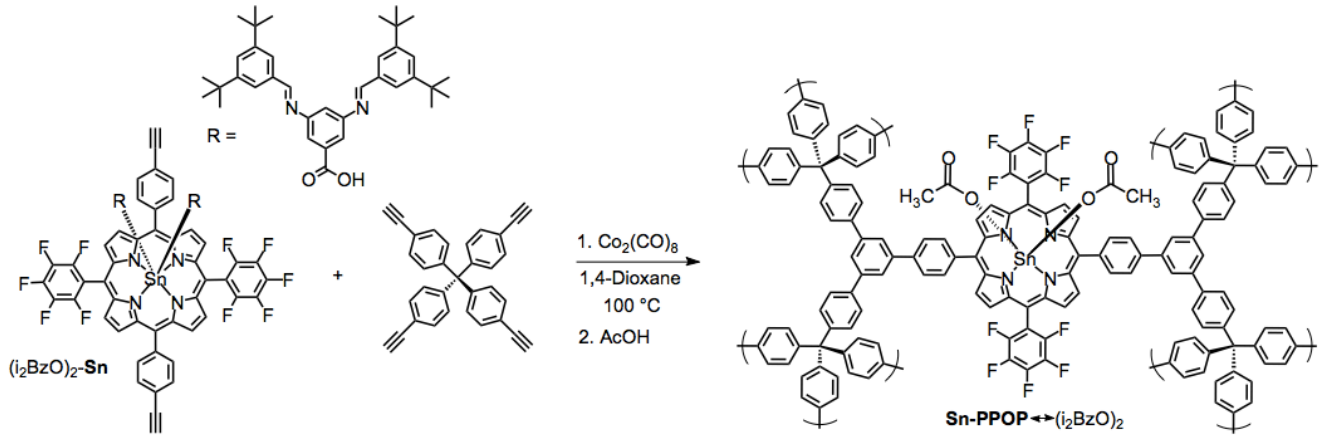

Sn-PPOP↔(i$_2$BzO)$_2$. **Sn-PPOP↔**(i$_2$BzO)$_2$ was synthesized under the same protocol and scale as described for **Sn-**

PPOP↔$(OH)_2$, but was worked up using aqueous acetic acid (2 mL of an AcOH:H_2O 1:1 v/v mixture). The complete release of the i_2BzOH ligand (95%) during the acetic acid workup was observe by GC analysis (see protocol described above for **Sn-PPOP↔(^{t}Bu$_2$BzO)$_2$**). Product was isolated as a purple solid (90 mg, 70% yield). Anal.: Calcd for $(C_{137}H_{68}F_{20}N_8O_8Sn_2)_n$: C, 63.99; H, 2.67; N, 4.36. Found: C, 63.61; H, 3.12; N, 5.87. ICP-OES: Calcd for $(C_{137}H_{68}F_{20}N_8O_8Sn_2)_n$: 9.2 wt% Sn. Found: 9.2 wt% Sn.

S6. Non-lability of the axial ligands during Sn-PPOP synthesis. For the synthesis of **Sn-PPOP↔(^{t}Bu$_2$BzO)$_2$** and **Sn-PPOP↔(i_2BzO)$_2$**, the non-lability of the initial axial ligands was monitored by gas chromatography (GC) as follows. Periodically, the reaction vial was removed from the oil bath, a small aliquot (10 μl) of the supernatant liquid was quickly drawn through the septa of the crimp cap using a gas-tight syringe, and the reaction vial was then placed back in the oil bath. The sampled aliquot was diluted with a solution of biphenyl in CH_2Cl_2 (1 mL of a 2 mM solution) and the resulting solution was analyzed by GC for the presence of axial ligand (3,5-di-*tert*-butyl benzoic acid for **Sn-PPOP↔(^{t}Bu$_2$BzO)$_2$** or i_2BzOH (also its degradation products 3,5-diaminobenzoic acid and 3,5-di-*tert*-butyl benzaldehyde) for **Sn-PPOP↔(i_2BzO)$_2$**) against the biphenyl external standard. No axial ligands were observed by GC analysis, confirming their non-lability during the polymerization.

S7. Preparation of supercritical CO_2-processed ^{scp}Sn-PPOPs.

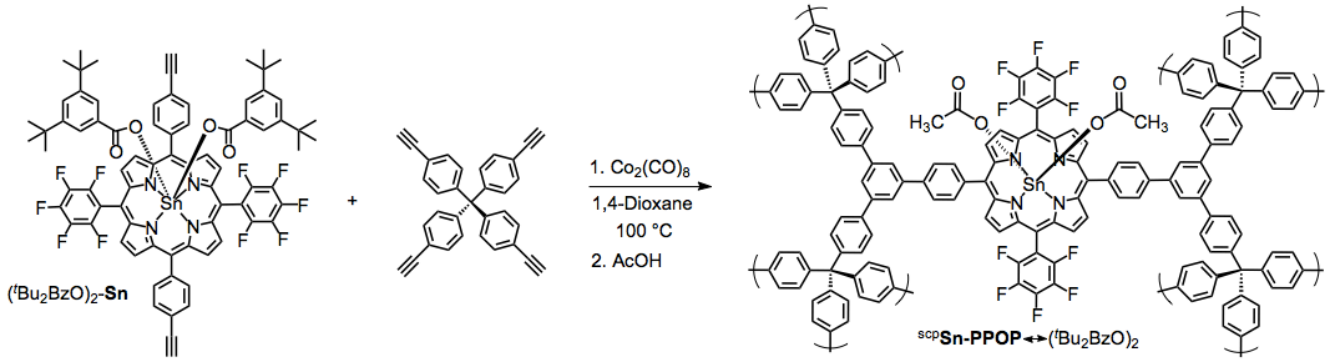

^{scp}Sn-PPOP↔(^{t}Bu$_2$BzO)$_2$. **Sn-PPOP↔(^{t}Bu$_2$BzO)$_2$** was synthesized under the same protocol and scaled up as described in section S5 but was worked up differently after the acetic acid quenching step. At this point, the hot reaction mixture was filtered over a fine-fritted glass funnel and the remaining purple solid was rinsed thoroughly with absolute ethanol (~100 mL), taking care to continually keep a layer of ethanol over the solid (it is critical to never allow the polymer sample to dry in air as it will irreversibly shrink). The remaining fine slush was transferred into an 8 dram vial by pipette, using ethanol to complete the transfer, bringing the total volume to 20 mL. This suspension was allowed to stir overnight at room temperature before being poured into a fine-fritted glass filter; the remained purple solid was rinsed thoroughly with ethanol (~50 mL), again with care being taken to continually keep a layer of ethanol over the solid.

The remaining fine slush was again transferred into a 20 mL scintillation vial by pipette, using ethanol to complete transfer; however, the total volume was kept to about 2 mL. The vial was then placed inside a Tousimis™ Samdri® PVT-30 critical point dryer (Tousimis, Rockville, MD) that has been retrofitted to fit the 20 mL vial. The ethanol was then exchanged with supercritical liquid CO_2 (maintained at ~ 0-10 °C) over a period of 8 h. Every hour, the liquid CO_2 was vented under positive pressure for 2 minutes (most of liquid have been evaporated after 30 s), taking care to maintain the rate of venting below the rate of filling so that the drying chamber remains full. After 8 h, the temperature inside the sealed chamber was raised to 38 ºC, which increased the pressure to above the critical point of CO_2 at 1300 psi. This pressure was maintained for 30 minutes, then the chamber was slowly vented over a period of 12 h while being kept at 38 ºC. The dried sample was tested for nitrogen adsorption immediately. Anal.: Calcd for $(C_{137}H_{68}F_{20}N_8O_8Sn_2)_n$: C, 63.99; H, 2.67; N, 4.36. Found: C, 61.02; H, 2.62; N, 4.22.

Note: If supercritical CO_2-processed Sn-PPOPs are exposed to organic solvents (i.e., dichloromethane, methanol) and then allowed to dry, the solvent-exposed sample will irreversibly shrink and lose some of its porosity. See section S13 below for more details.

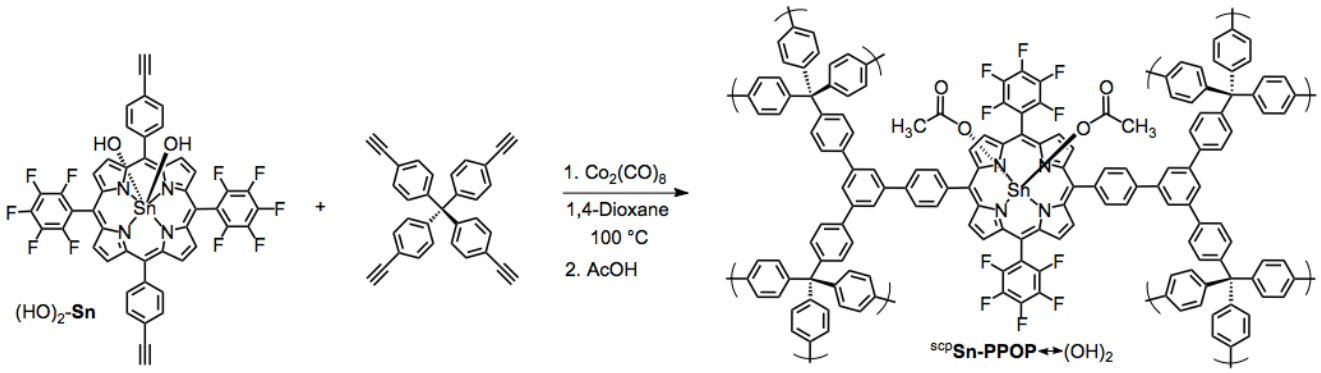

^{scp}Sn-PPOP↔(OH)$_2$. **Sn-PPOP↔**(OH)$_2$ was synthesized under the same protocol and scale as described in section S5 and processed with supercritical CO_2 as detailed for ^{scp}**Sn-PPOP↔**(^{t}Bu$_2$BzO)$_2$. Anal.: Calcd for $(C_{137}H_{68}F_{20}N_8O_8Sn_2)_n$: C, 63.99; H, 2.67; N, 4.36. Found: C, 58.27; H, 2.28; N, 4.22.

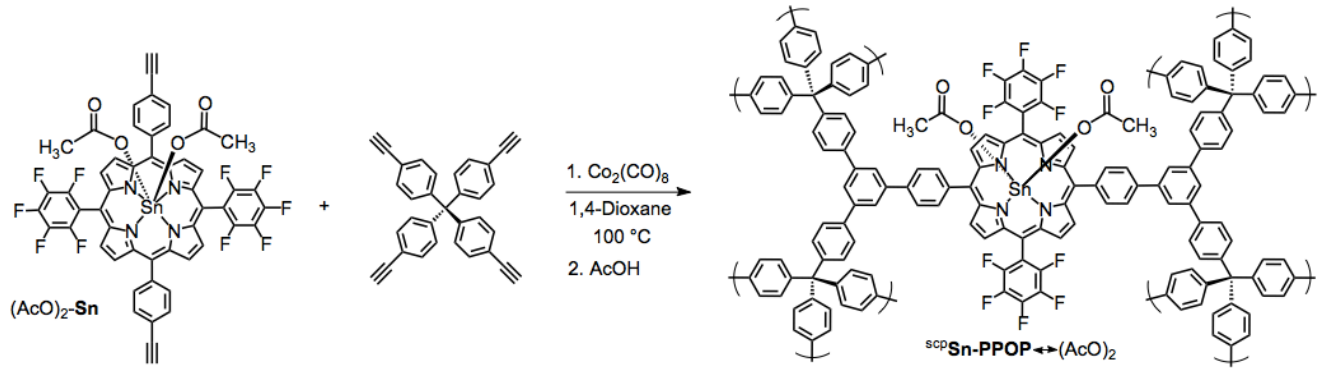

^{scp}Sn-PPOP↔(AcO)$_2$. **Sn-PPOP↔**(AcO)$_2$ was synthesized under the same protocol and scale as described in section S5 and processed with supercritical CO_2 as detailed for ^{scp}**Sn-PPOP↔**(^{t}Bu$_2$BzO)$_2$. Anal.: Calcd for $(C_{137}H_{68}F_{20}N_8O_8Sn_2)_n$: C, 63.99; H, 2.67; N, 4.36. Found: C, 60.53; H, 2.54; N, 4.29.

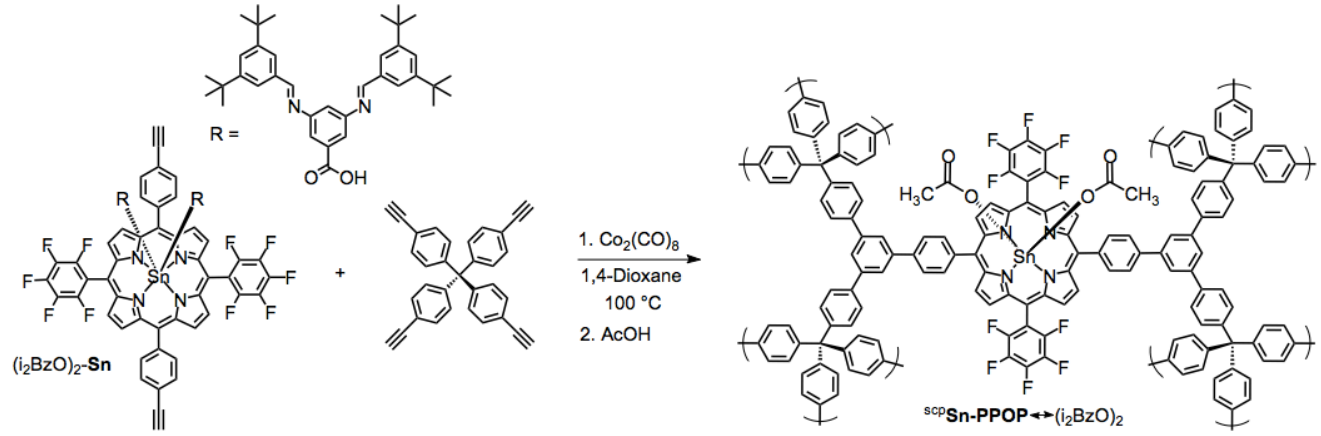

^{scp}Sn-PPOP↔(i$_2$BzO)$_2$. **Sn-PPOP↔**(i$_2$BzO)$_2$ was synthesized under the same protocol and scale as described in section S5 and processed with supercritical CO_2 as detailed for ^{scp}**Sn-PPOP↔**(^{t}Bu$_2$BzO)$_2$. Anal.: Calcd for $(C_{137}H_{68}F_{20}N_8O_8Sn_2)_n$: C, 63.99; H, 2.67; N, 4.36. Found: C, 61.43; H, 2.41; N, 4.37. See Fig. S10 for the solid-state ^{1}H-^{13}C CP-MAS NMR spectrum.

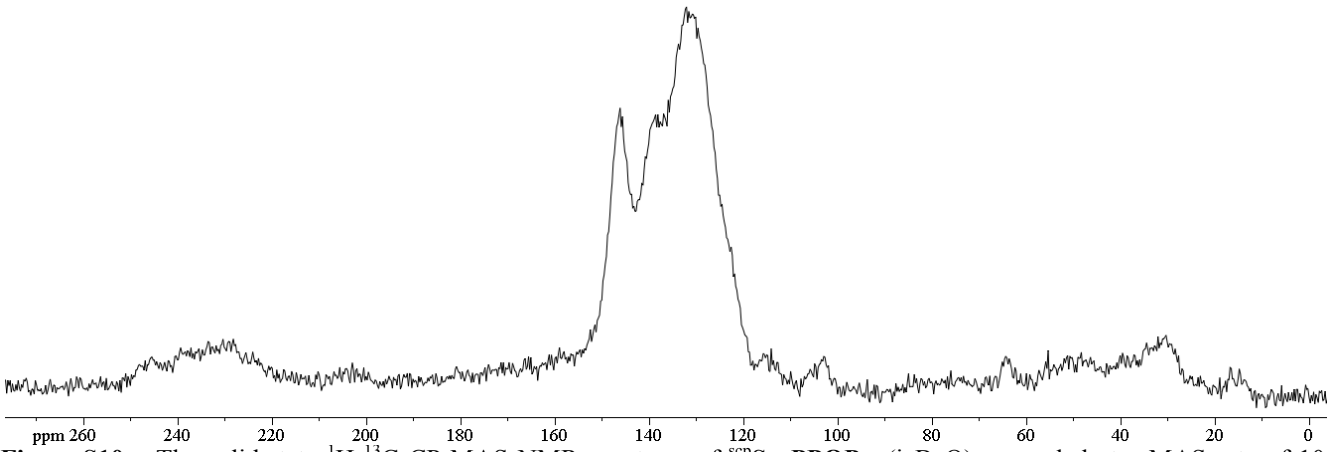

Figure S10. The solid-state ^{1}H-^{13}C CP-MAS NMR spectrum of ^{scp}**Sn-PPOP**↔$(i_2BzO)_2$ recorded at a MAS rate of 10 kHz.

S8. N_2 isotherm of $(^tBu_2BzO)_2$Sn-PPOP before acetic acid workup.

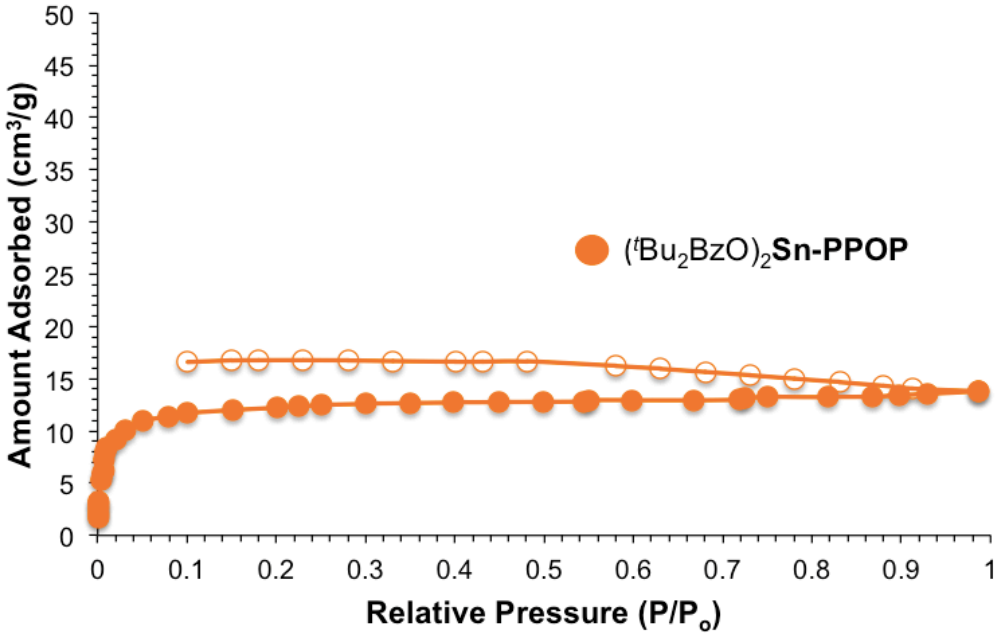

Figure S11. The N_2 isotherm of $(^tBu_2BzO)_2$**Sn-PPOP** before acetic acid work up, recorded at 77 K. Closed symbols = adsorption; open symbols = desorption. BET surface area: 50 m^2/g; total pore volume: 0.02 cm^3/g; total micropore volume: 0.02 cm^3/g; dominant pore diameter: 12, 15 Å.

S9. N_2 isotherm and pore size distribution of Sn-PPOP↔$(i_2BzO)_2$.

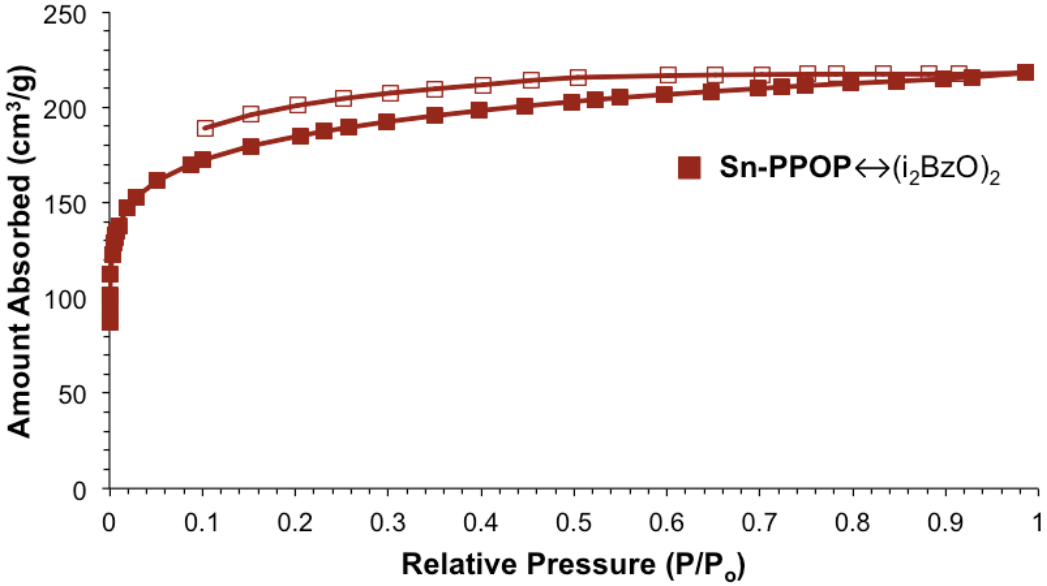

Figure S12. The N_2 isotherm of **Sn-PPOP**↔$(i_2BzO)_2$ recorded at 77 K. Closed symbols = adsorption; open symbols = desorption. BET surface area: 620 m^2/g; total pore volume: 0.29 cm^3/g; total micropore volume: 0.21 cm^3/g; dominant pore diameter: 10, 12, 15, 21, 27 Å.

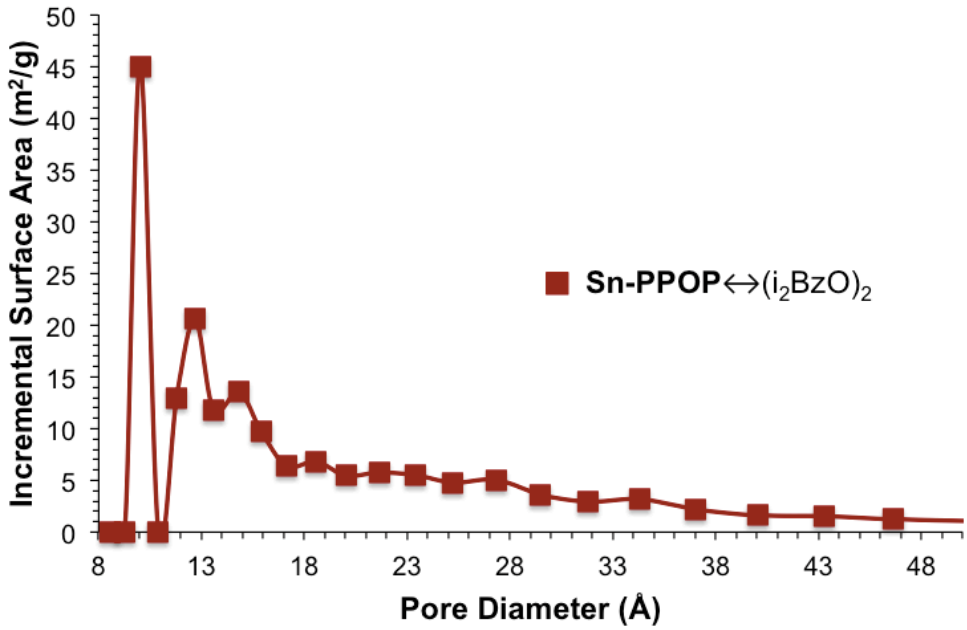

Figure S13. The pore size distribution plot for **Sn-PPOP**↔$(i_2BzO)_2$ according to DFT analysis of the N_2 adsorption isotherm.

S10. N_2 isotherms and pore size distribution profiles of ^{scp}Sn-PPOP↔$(OH)_2$, ^{scp}Sn-PPOP↔$(AcO)_2$, ^{scp}Sn-PPOP↔$(^tBu_2BzO)_2$, and ^{scp}Sn-PPOP↔$(i_2BzO)_2$.

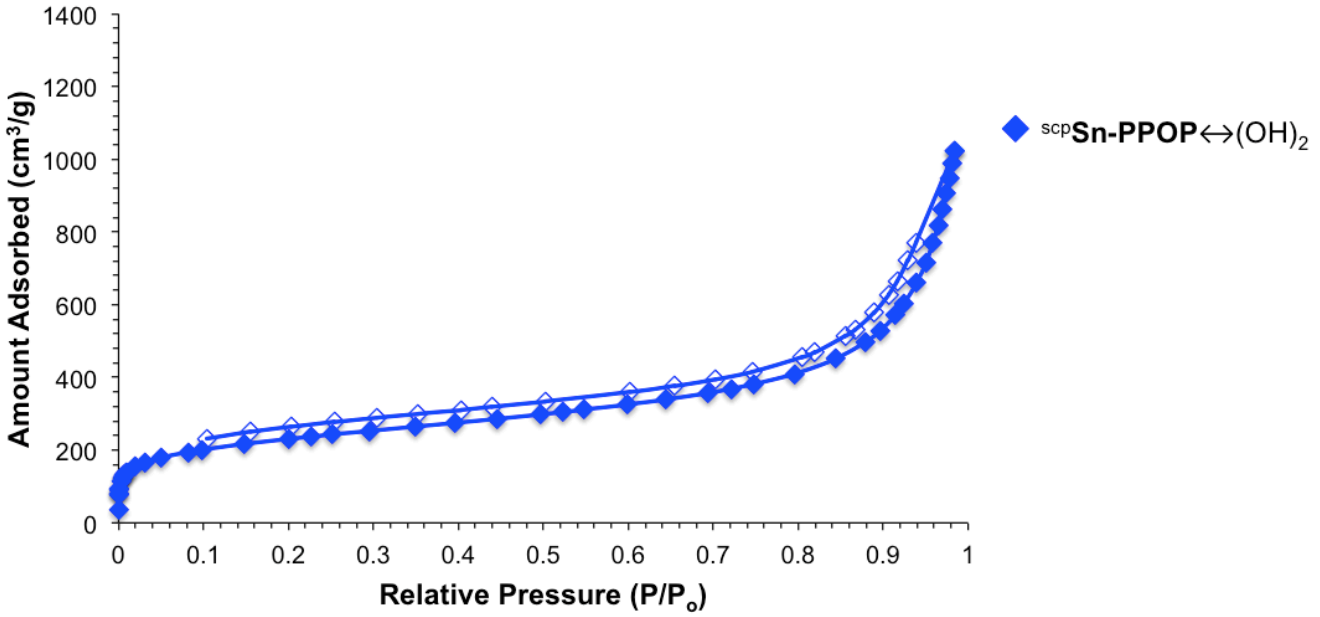

Figure S14. The N_2 isotherm of ^{scp}**Sn-PPOP**↔$(OH)_2$ recorded at 77 K. Closed symbols = adsorption; open symbols = desorption.

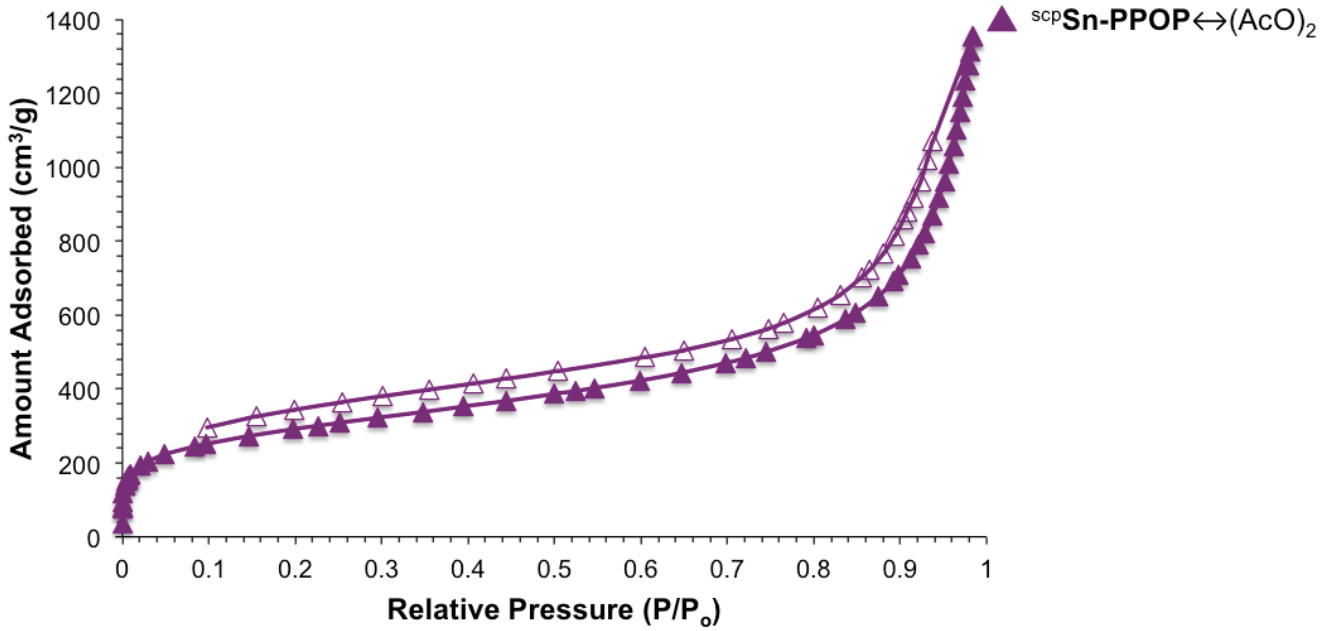

Figure S15. The N_2 isotherm of ^{scp}**Sn-PPOP**↔$(AcO)_2$ recorded at 77 K. Closed symbols = adsorption; open symbols = desorption.

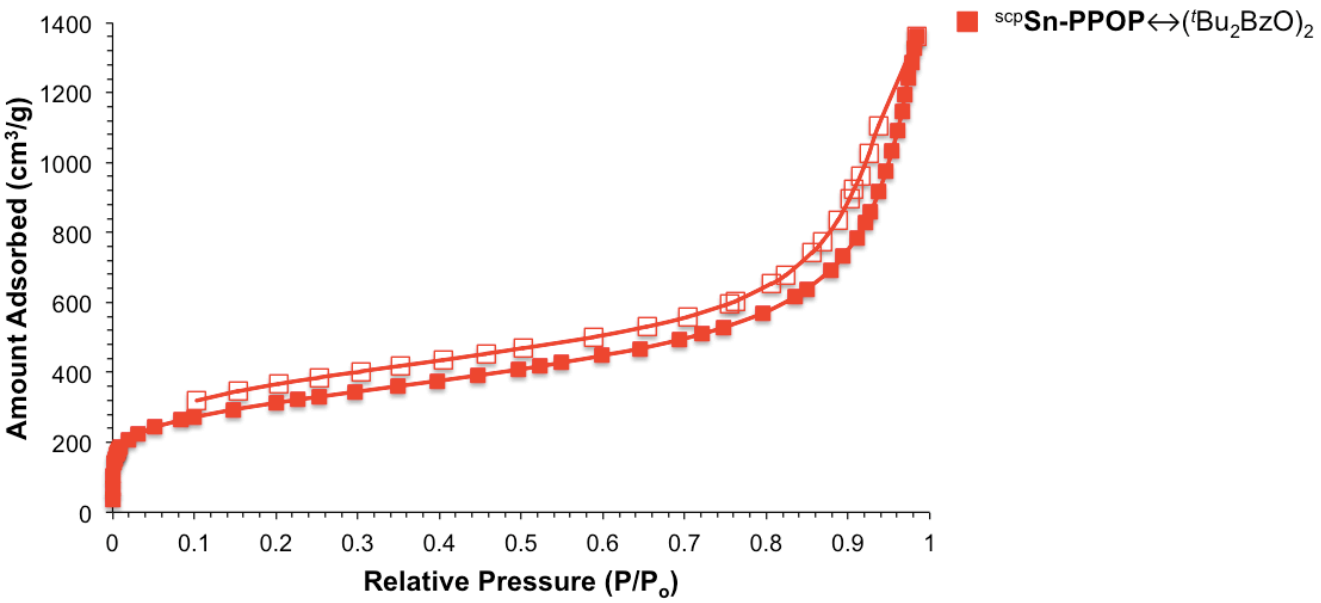

Figure S16. The N_2 isotherm of ^{scp}**Sn-PPOP**↔(^{t}Bu$_2$BzO)$_2$ recorded at 77 K. Closed symbols = adsorption; open symbols = desorption.

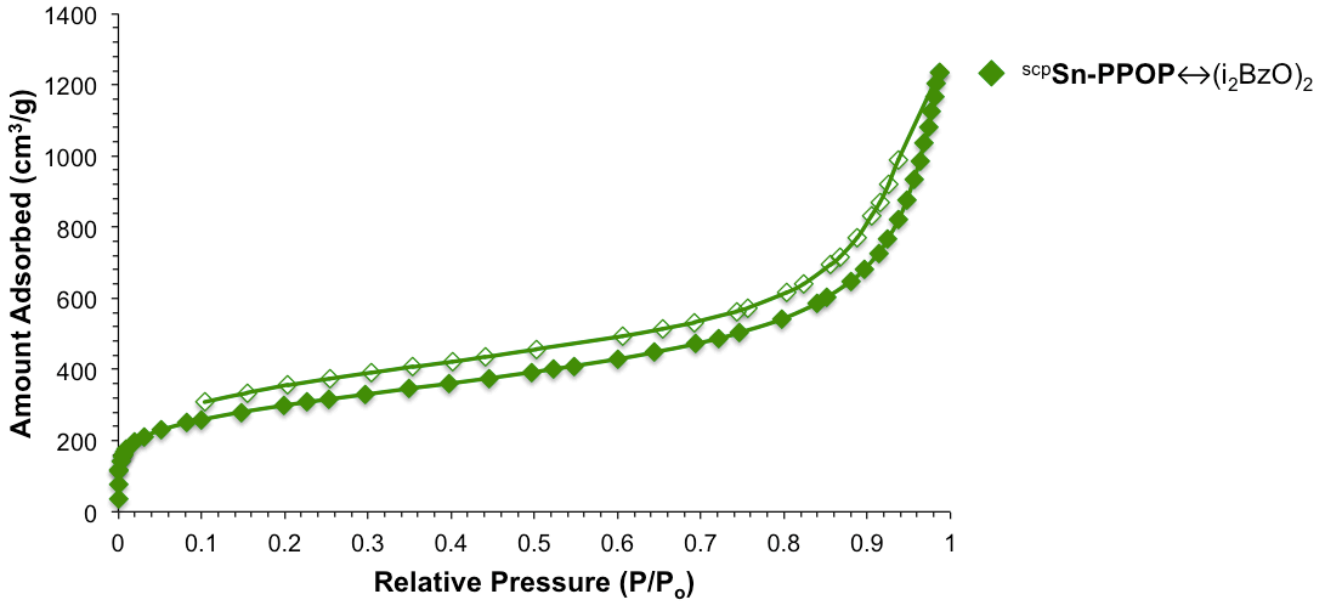

Figure S17. The N_2 isotherm of ^{scp}**Sn-PPOP**↔(i$_2$BzO)$_2$ recorded at 77 K. Closed symbols = adsorption; open symbols = desorption.

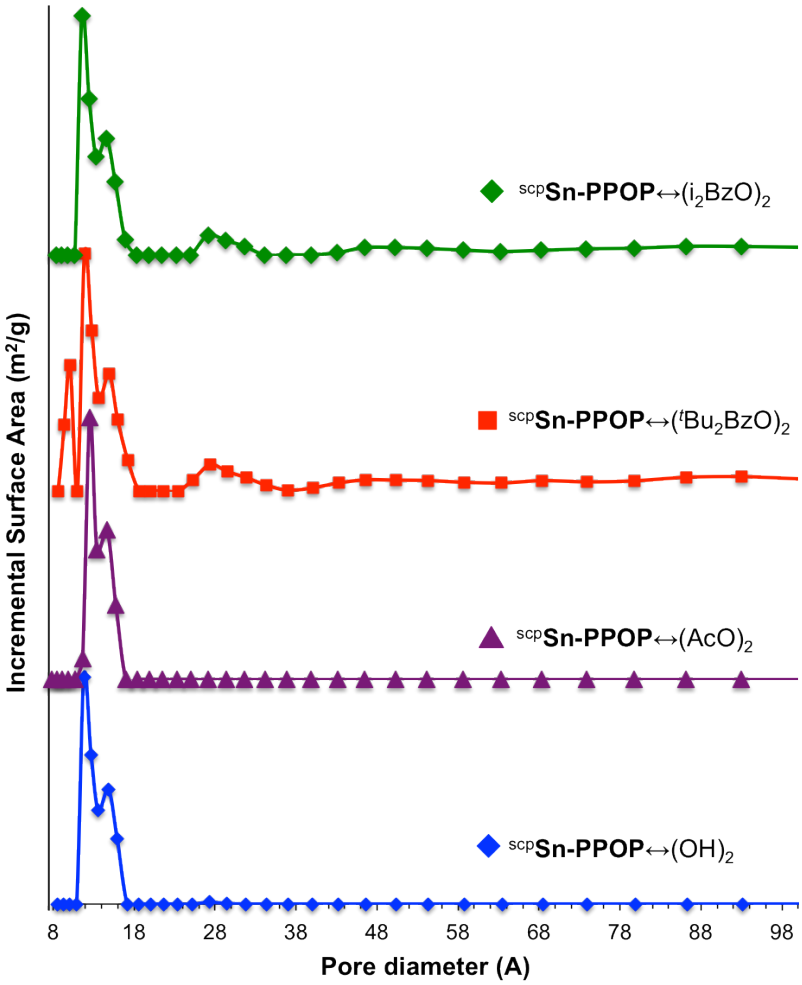

Figure S18. The pore size distribution plots for ^{scp}**Sn-PPOP**↔$(OH)_2$, ^{scp}**Sn-PPOP**↔$(AcO)_2$, ^{scp}**Sn-PPOP**↔$(^tBu_2BzO)_2$, and ^{scp}**Sn-PPOP**↔$(i_2BzO)_2$ according to DFT analysis of the N_2 adsorption isotherms.

S11. Stacked solid-state NMR plot.

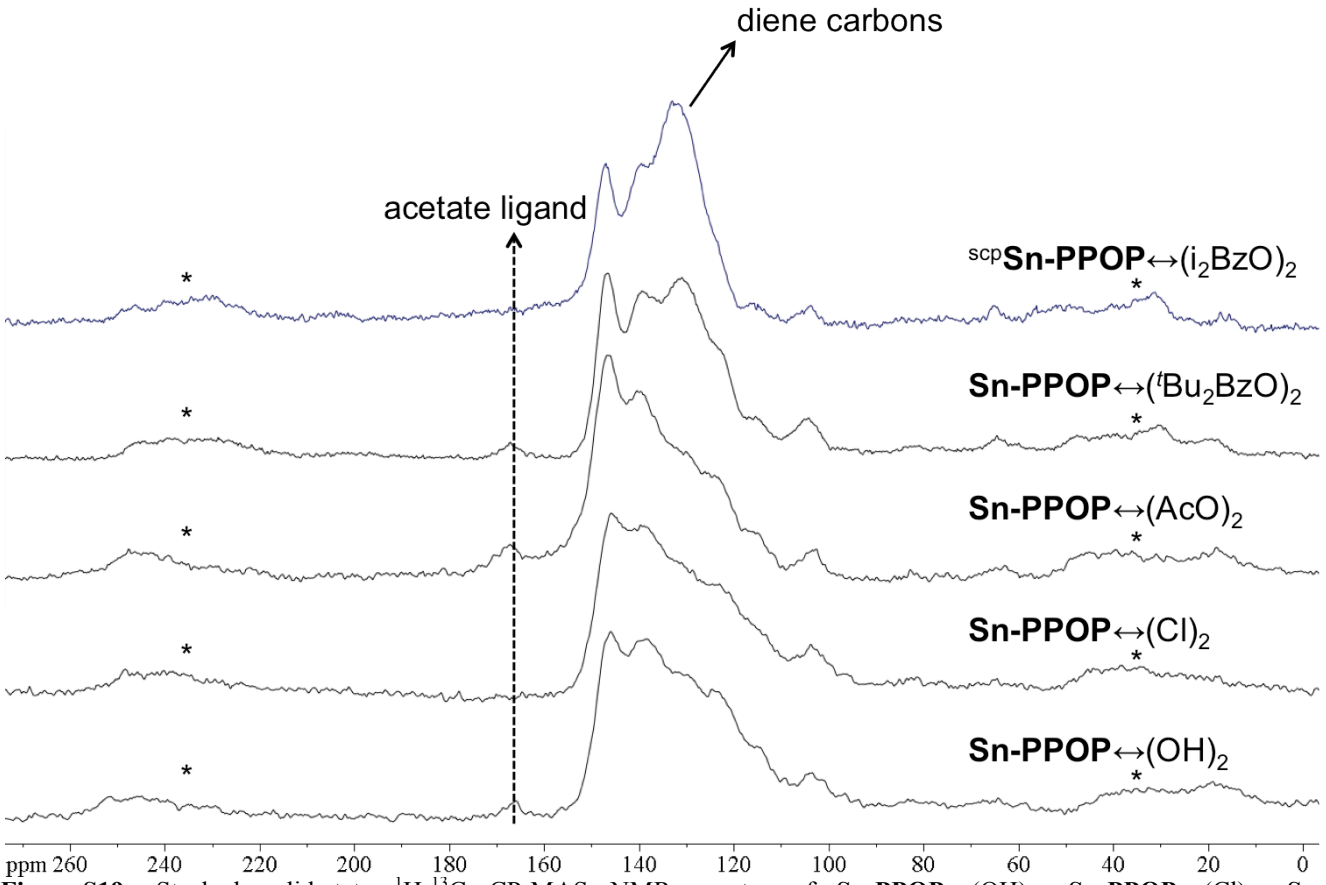

Figure S19. Stacked solid-state ^{1}H-^{13}C CP-MAS NMR spectra of **Sn-PPOP↔**$(OH)_2$, **Sn-PPOP↔**$(Cl)_2$, **Sn-PPOP↔**$(AcO)_2$, **Sn-PPOP↔**$(^{t}Bu_2BzO)_2$, and ^{scp}**Sn-PPOP↔**$(i_2BzO)_2$ recorded at a MAS rate of 10 kHz. The absence of the resonance due to the acetate ligand in ^{scp}**Sn-PPOP↔**$(i_2BzO)_2$ can be attributed to its loss during the solvent exchange step with EtOH prior to supercritical CO_2 processing. Unfortunately, we cannot clearly distinguish the ethoxide resonance, if any is present, due to their overlap with the spinning side bands (indicated as *).

S12. Densities of supercritical CO_2-processed Sn-PPOPs. According to Lowell *et al.*,[S5] the *skeletal density* is the ratio of the mass to the volume occupied by the *framework* of the sample excluding the volume of any open pores while the *bulk density* is the ratio of the mass to the volume occupied by the *whole* sample, including all internal pore and interparticle void space (*pore volume*). Hence, the bulk density can be calculated if the measured skeletal density and the total pore volume of each material are known (Eq S1).

$$\rho_{bulk} = 1/[(1/\rho_{skeletal}) + V_{total\ pore}] \quad \text{(S1)}$$

Table S1. Densities of Sn-PPOP derivatives

Sn-PPOP derivatives	Total NLDFT-derived pore volume ($cm^3\ g^{-1}$)[a]	$\rho_{skeletal}$ ($g\ mL^{-1}$)[b]	NLDFT-derived ρ_{bulk} ($g\ mL^{-1}$)[c]
^{scp}**Sn-PPOP↔**$(OH)_2$	1.02	2.39	0.70
^{scp}**Sn-PPOP↔**$(AcO)_2$	1.13	2.29	0.64
^{scp}**Sn-PPOP↔**$(^{t}Bu_2BzO)_2$	1.42	1.64	0.49
^{scp}**Sn-PPOP↔**$(i_2BzO)_2$	1.27	1.69	0.54

[a]Total NLDFT-derived pore volume from the N_2 adsorption profiles at $p/p_0 = 0.98$. [b]Derived from helium pycnometry. Data is averaged from ten measurements with standard deviations of less than 0.01. [c]The bulk densities calculated using the NLDFT-derived pore volumes.

S13. Porosity of ^{scp}Sn-PPOP↔(AcO)$_2$ after dichloromethane exposure.

To determine the effect of organic solvent on the porosity of supercritical CO_2-processed Sn-PPOPs, a sample of ^{scp}**Sn-PPOP↔(AcO)$_2$** (50 mg) was suspended in CH_2Cl_2 (5 mL) in a vial for 6 h before being filtered. The resulting solvent-exposed material was then dried under vacuum overnight before BET measurements were obtained. As can be seen in the top panel of Figure S20 below, the porosity of this material is comparable to that of the thermally activated **Sn-PPOP↔(AcO)$_2$** sample (Table 1 in the main text, entry 3a) and is significantly decreased from that of ^{scp}**Sn-PPOP↔(AcO)$_2$** (Table 1 in the main text, entry 3b). Visually, ^{scp}**Sn-PPOP↔(AcO)$_2$** has "shriveled" up after exposure to the CH_2Cl_2 and vacuum-drying. As in the case of the thermally activated **Sn-PPOP↔(AcO)$_2$** sample, we attributed this to an irreversible loss of the "interparticle" mesopores, and a subsequent loss in surface area and pore volume. We note that further thermal activation of the vacuum-dried, solvent-exposed ^{scp}**Sn-PPOP↔(AcO)$_2$** does not lead to any change in surface area (Figure S20, bottom panel)

We note however that porphyrin-derived POPs that have been processed with supercritical CO_2 can be reactivated to their original high porosities after being exposed to common organic solvents, as we have previously demonstrated in the recycling of catalytically active Al(porphyrin)-derived POPs.[S6] By exchanging the organic media of the catalytic reaction with ethanol, the solvent-wetted Al(porphyrin) POPs can be reprocessed again via supercritical CO_2 to regain their original high porosities.

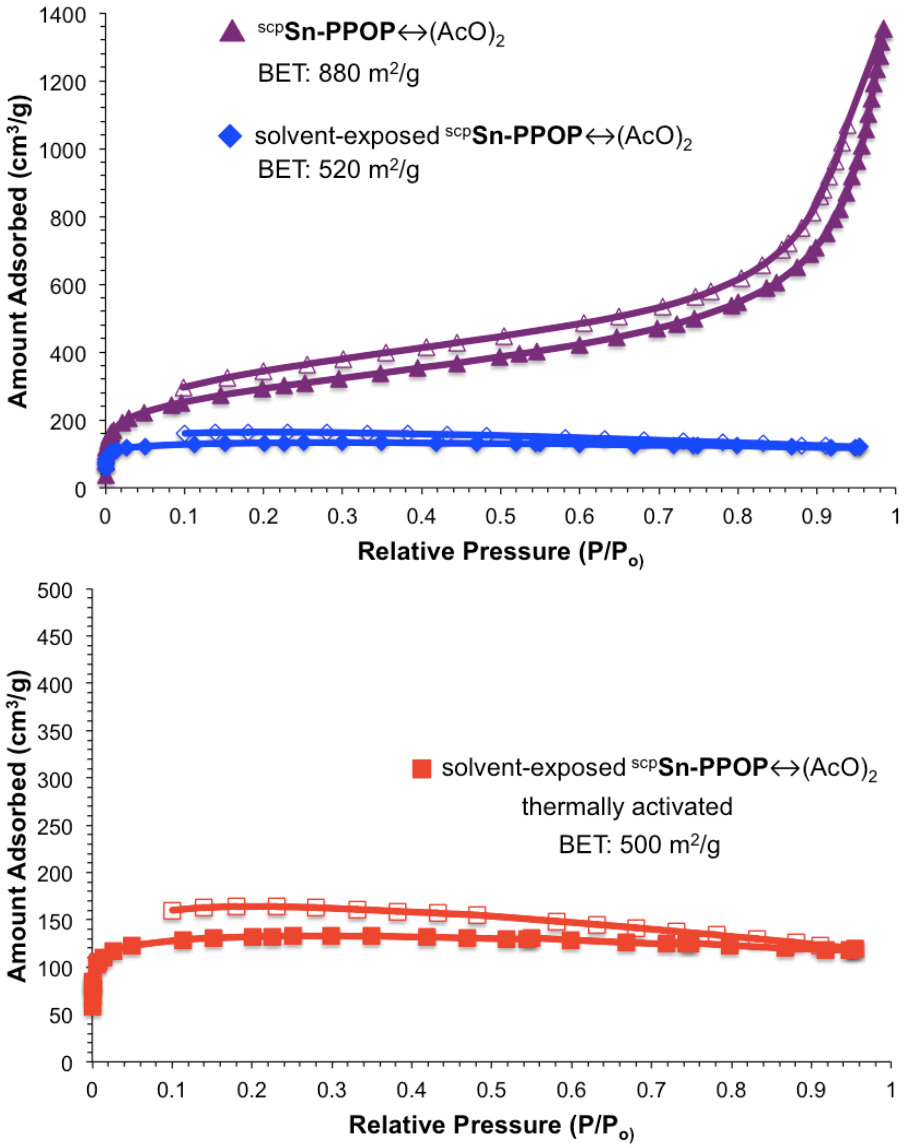

Figure S20. Top: The N_2 isotherms of ^{scp}**Sn-PPOP↔(AcO)$_2$** recorded at 77 K before and after exposure to CH_2Cl_2. Bottom: The N_2 isotherm of the vacuum-dried, solvent-exposed ^{scp}**Sn-PPOP↔(AcO)$_2$** recorded at 77 K after thermal activation. Closed symbols = adsorption; open symbols = desorption.

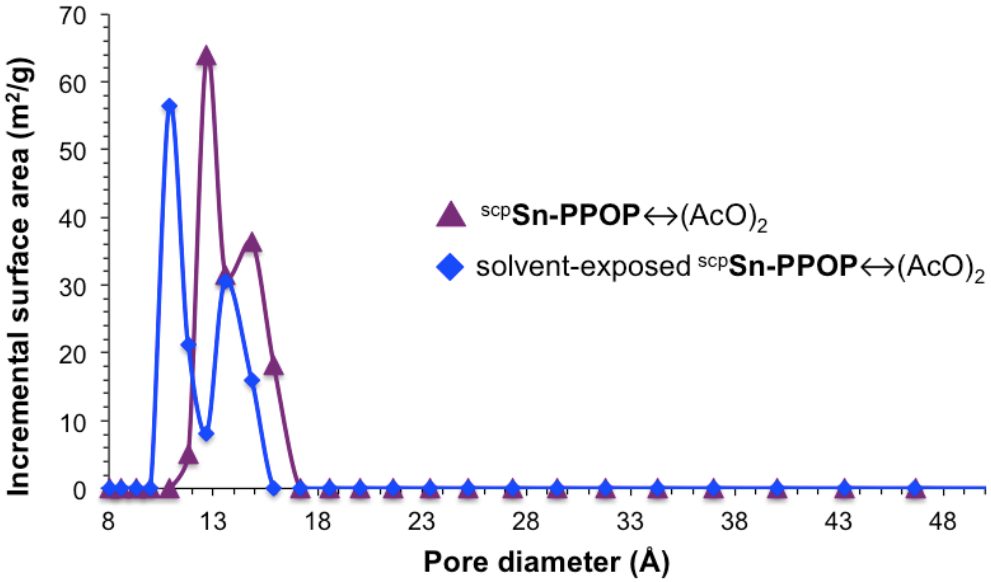

Figure S21. The pore size distribution plots for ^{scp}**Sn-PPOP**↔$(AcO)_2$, and solvent-exposed ^{scp}**Sn-PPOP**↔$(AcO)_2$ according to DFT analysis of the N_2 adsorption isotherms.

S14. SEM images of Sn-PPOPs. As seen in Figures S22, S25, and S26 below (data are for the [**Sn-PPOP**↔$(OH)_2$ and ^{scp}**Sn-PPOP**↔$(OH)_2$], [**Sn-PPOP**↔$(^tBu_2BzO)_2$ and ^{scp}**Sn-PPOP**↔$(^tBu_2BzO)_2$], and [**Sn-PPOP**↔$(i_2BzO)_2$ and ^{scp}**Sn-PPOP**↔$(i_2BzO)_2$] pairs, respectively), the average particle size of our POPs appear to be quite smaller after supercritical CO_2 processing, as expected from our hypothesis that supercritical CO_2 processing preserves the void volumes between the polymer particles and decrease their aggregation.

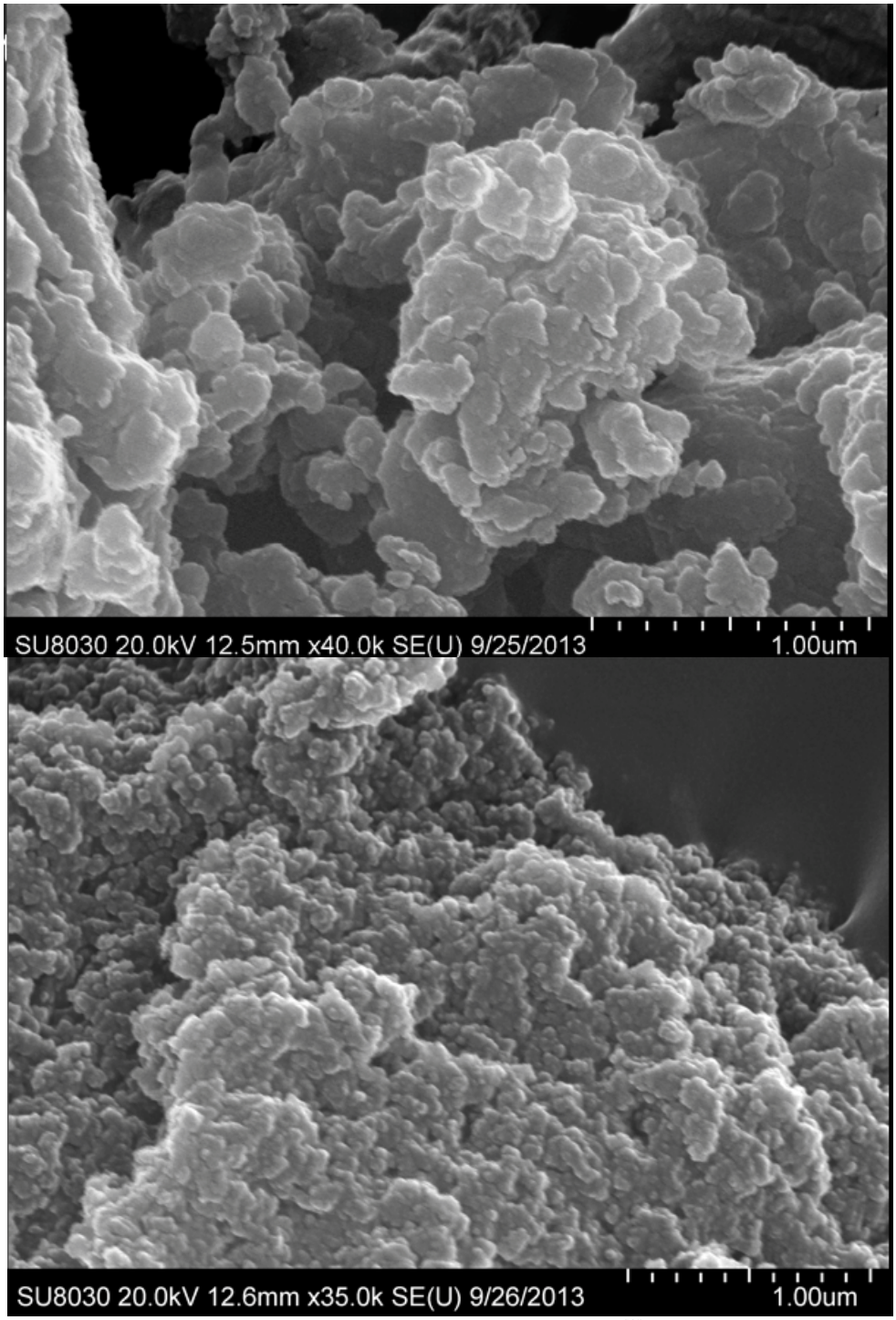

Figure S22. SEM images of thermally activated **Sn-PPOP**↔$(OH)_2$ (top) and ^{scp}**Sn-PPOP**↔$(OH)_2$ (bottom).

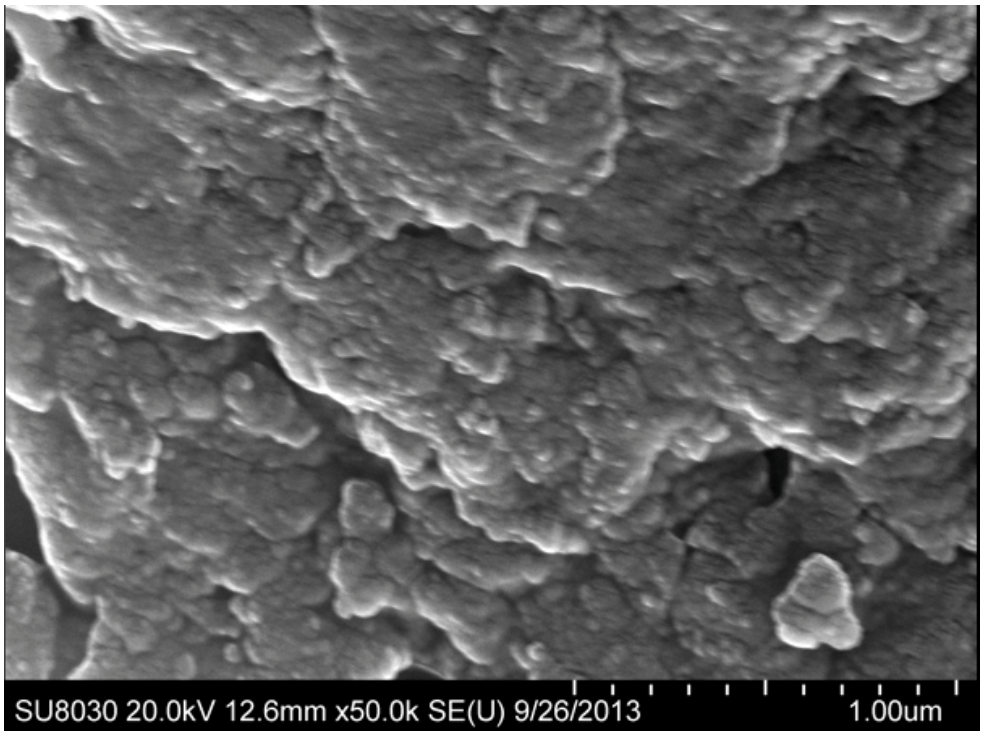

Figure S23. SEM image of thermally activated **Sn-PPOP↔**$(Cl)_2$

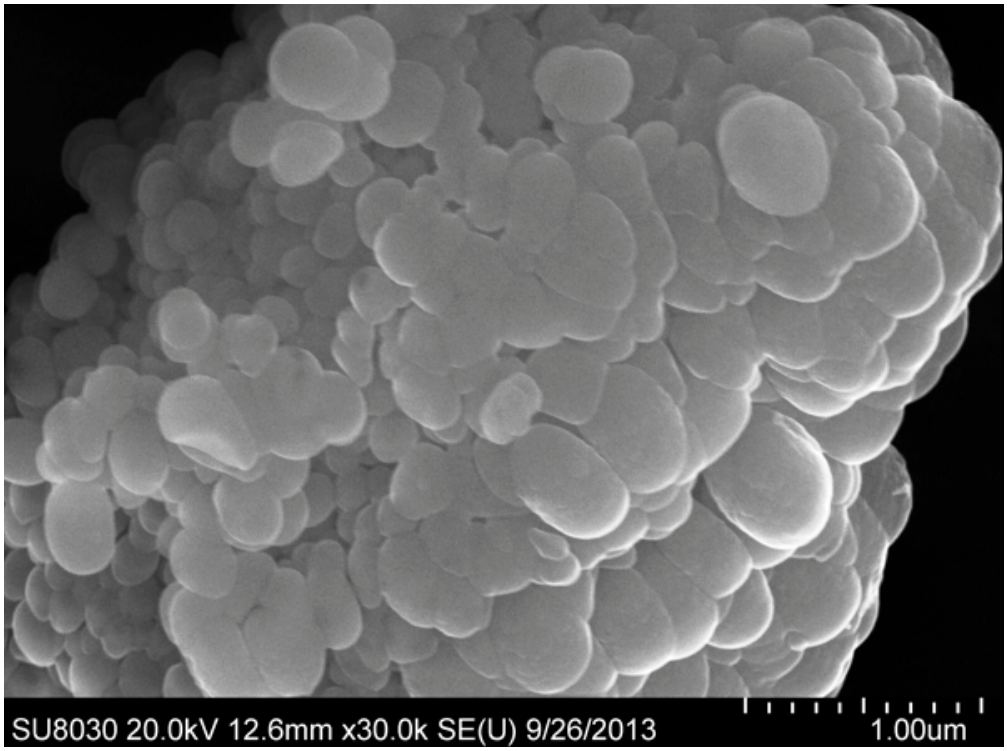

Figure S24. SEM image of thermally activated **Sn-PPOP↔**$(AcO)_2$

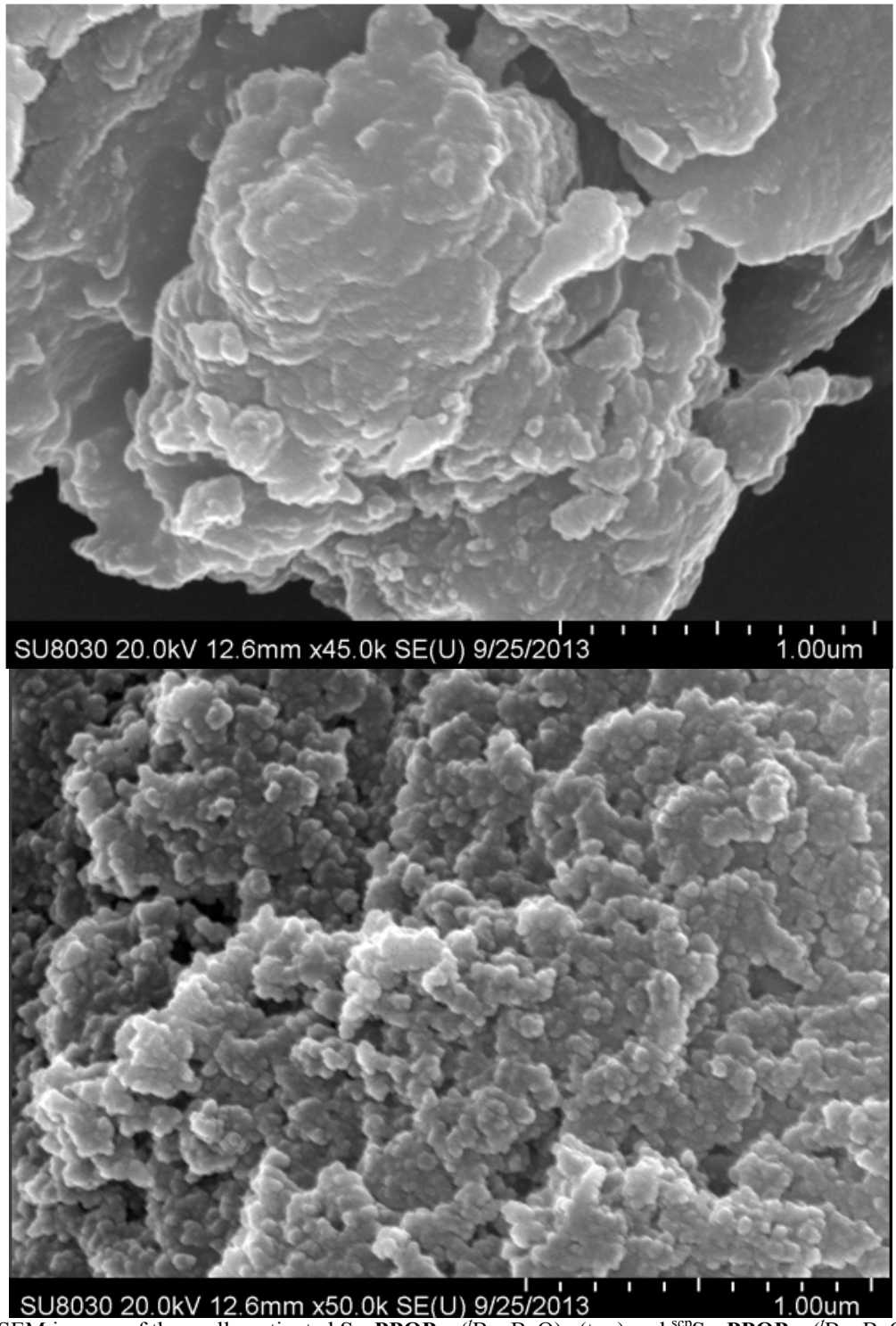

Figure S25. SEM images of thermally activated **Sn-PPOP**↔(^{t}Bu$_2$BzO)$_2$ (top) and ^{scp}**Sn-PPOP**↔(^{t}Bu$_2$BzO)$_2$ (bottom).

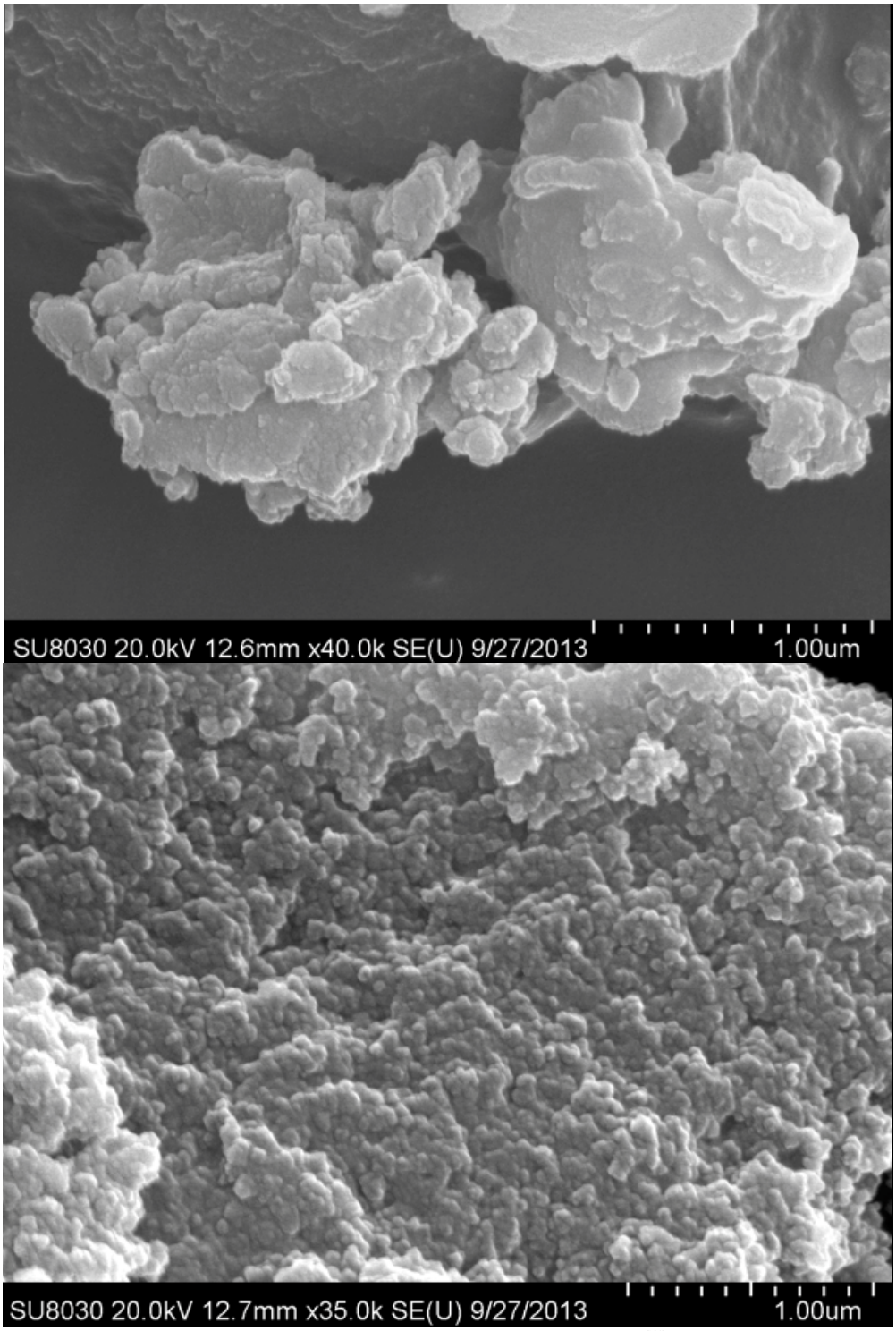

Figure S26. SEM images of thermally activated **Sn-PPOP**↔$(i_2BzO)_2$ (top) and ^{scp}**Sn-PPOP**↔$(i_2BzO)_2$ (bottom)

S15. Authors contribution audit. R.K.T., O.K.F., J.T.H., and S.T.N. conceived the experiments presented herein. R.K.T, L.L.O., and Y.S.K. synthesized all compounds with the exception of *tetrakis*(4-ethynylphenyl)methane, which was synthesized by M.H.W. R.K.T. and L.L.O. carried out the characterization of all polymers. S.C. obtained the SEM images of the POPs and carried out the solvent-exposed study described in section S13. R.K.T. conducted the supercritical CO_2 activation. O.K.F., J.T.H., and S.T.N. supervised the project. R.K.T. wrote the initial draft of the paper with inputs and corrections from all co-authors. R.K.T. and S.T.N. finalized the manuscript.

S16. References.

S1. A. B. Pangborn, M. A. Giardello, R. H. Grubbs, R. K. Rosen and F. J. Timmers, *Organometallics*, 1996, **15**, 1518-1520.
S2. P. Thamyongkit and J. S. Lindsey, *J. Org. Chem.*, 2004, **69**, 5796-5799.
S3. P. Pandey, O. K. Farha, A. M. Spokoyny, C. A. Mirkin, M. G. Kanatzidis, J. T. Hupp and S. T. Nguyen, *J. Mater. Chem.*, 2011, **21**, 1700-1703.
S4. J. K. Laha, S. Dhanalekshmi, M. Taniguchi, A. Ambroise and J. S. Lindsey, *Org. Process Res. Dev.*, 2003, **7**, 799-812.
S5. S. Lowell, J. E. Shields, M. A. Thomas and M. Thommes, *Characterization of Porous Solids and Powders: Surface Area, Pore Size, and Density,* 4th ed., Kluwer Academic, Dordrecht (The Netherlands), 2004.
S6. R. K. Totten, Y.-S. Kim, M. H. Weston, O. K. Farha, J. T. Hupp and S. T. Nguyen, *J. Am. Chem. Soc.*, 2013, **135**, 11720-11723.